Definition of a new set of parameters for the dynamic thermal characterization of PCM layers in the presence of one or more liquid-solid interfaces

D. Mazzeo[a,*], G. Oliveti[a], N. Arcuri[a]

Department of Mechanical, Energy and Management Engineering (DIMEG) - University of Calabria
P. Bucci 46/C - 87036 - Rende (CS) - Italy

*Corresponding author. Domenico Mazzeo, email address: domenico.mazzeo@unical.it, tel.: +39 0984 494605, fax: +39 0984 494673, address: Department of Mechanical, Energy and Management Engineering (DIMEG) - University of Calabria P. Bucci 46/C - 87036 - Rende (CS) - Italy

Abstract

The objective of the research is the definition of a new set of parameters to evaluate the effective dynamic thermal behavior of a layer subject to phase change (PCM) that, for the effect of non-sinusoidal periodic boundary conditions, characterizing the external walls of air-conditioned buildings, give rise to the formation of one or more melting or solidification bi-phase interfaces. Such bi-phase interfaces originate on the boundary surfaces, or are always present and fluctuate within the layer. Defined parameters are to be used for the thermal design of innovative walls containing a PCM layer, targeting the reduction of power peaks entering the environment, or in order to reduce the energy requirements or even to improve the indoor thermal comfort.

The study has been developed by a finite difference numeric calculation model, which explicitly determines, the number and the position of the bi-phase interfaces that originate in the layer and the temperature and the heat flux fields.

The methodology developed allowed us to determine the dynamic characteristics, for each month of the year, of PCM layers with different melting temperatures and thermo-physical properties and subject to climatic conditions of two locations, one with a continental climate and the second one with a Mediterranean climate. In particular, it was found that all defined dynamic parameters, irrespective of locality and of PCM type, are related to the latent storage efficiency and, furthermore, some calculation correlations between the dynamic parameters were obtained.

Finally, the results show that it was sufficient to reach the phase change in a portion of the layer of about 35% to obtain excellent dynamic thermal performance.

Keywords: phase change material; latent heat; building wall; dynamic thermal behavior; dynamic parameters; bi-phase interface; Stefan problem; energy efficiency; passive system; melting temperature; continental climate; mediterranean climate

1. Introduction

Phase change material (PCM) has been widely employed in building envelopes with the aim of reducing and shifting the heating and cooling load peak, allowing for smaller dimensions of air-

conditioning plants, to reduce energy requirements, and to maintain a more comfortable indoor environment due to smaller temperature fluctuations [1-13]. The presence of a phase change material (PCM) layer in an air-conditioned building wall, due to the effect of storage and release of latent energy phenomena, modifies the dynamic thermal behavior, both during the summer and winter periods.

The building external walls are subject, on the outside surface, to the action of solar radiation, as well as that of air temperature and apparent sky temperature. On the internal surface they are subject to thermal exchanges, convective with the air, infrared radiative with other walls and to the absorbed solar radiation that penetrates through the glazed surfaces. The variability of such loadings can be schematized by non-sinusoidal periodical fluctuations, which in the outdoor environment are representative of the average monthly day of the thermal quantities, and which cause a steady periodic thermal regime in the layer after an initial thermal transient. In such a regime, upon variability of the boundary conditions in relation to the PCM melting temperature, one or more bi-phase interfaces can originate, which are formed on the external surface or also on the internal surface, and that involve a part of the layer or the entire layer. It may occur that the layer is not subject to phase change and it remains in a solid or liquid phase. The storage and the release processes of latent energy at the melting temperature, compared to the monophase layer, give rise to an abrupt modification of the thermal fluctuations on the external and internal surfaces. For such a reason, the dynamic characterization of a PCM layer, unlike a monophase layer, requires the definition of a new set of parameters that identify dynamic thermal and energetic behavior.

In a monophase layer in periodic sinusoidal conditions, the dynamic characterization is obtained by: the periodic thermal transmittance, the thermal admittances, the areal heat capacities, the decrement factor and the time lag of the periodic thermal transmittance, determined by the consideration of the air temperature as external loading and the temperature of the environment, supposed as constant, as the internal loading [14]; the surface factor evaluated in the presence of a heat flux oscillation on the internal surface and with the air temperature on both faces of the wall maintained constant [15]; the non-dimensional periodic thermal transmittance and the periodic heat storage efficiency in the presence of more loadings which act on the external and internal face [16, 17]. In non-sinusoidal periodic conditions, the dynamic parameters considered are: the decrement factor of energy, the decrement factor and the time lag of the maximum and the minimum peak of the heat flux calculated in the presence of more loadings which act on the external and internal surface [16-18]; the decrement factor of the daily maximum excursion and the time lag of the maximum peak and the minimum peak of the temperature considering the actual sol-air temperature as the external loading and considering constant the indoor air temperature [19]; the conventional periodic thermal transmittance corrected by a factor evaluated considering the actual sol-air temperature as the external loading and considering constant the indoor air temperature [20].

For the dynamic characterization of a PCM layer, new parameters have been proposed in the scientific literature. In a sinusoidal periodic regime, Zhou et al. [21, 22] have studied the effects of PCM thermophysical properties, inner surface convective heat transfer coefficient and thickness of a PCM wallboard on the time lag, decrement factor and phase transition keeping time of the inner surface when the layer is subjected to the action of a periodic sinusoidal temperature or heat flux on the outer surface. Sharifi et al. [23] have used the decrement factor and the time lag, in sinusoidal temperature conditions, and the duration of being in the comfort zone and the energy required to keep the inside temperature in the comfort zone, in a dynamic regime, to evaluate the dynamic behavior of a based PCM-impregnated gypsum board. Ling et al. [24] have proposed and evaluated three indicators, namely, thermal storage coefficient, thermal resistance and thermal inertia index of PCM useful in evaluating the thermal inertia performance of a building component with PCM heated with periodic fluctuation. Evola et al. [25] have introduced a series of indicators in dynamic regime that allow a precise description of both the PCM behavior (frequency of melting, storage efficiency) and the intensity and duration of the thermal comfort perceived by occupants. In the same thermal regime, Ye et al. [26] have evaluated the ESI, the ratio of a particular material or component's energy saving equivalent (ESE) to the corresponding value of the ideal material or component that can maintain the room at an ideal thermal state in passive mode, where the ESE represents the hypothetical energy to be supplied to maintain a passive room at the same thermal state as that when a particular material or component is adopted. Sun et al. [27] have proposed the energy and mass efficiency (EME), an index which considers the melting temperature and PCM layer thickness and the outdoor and indoor air temperature, to evaluate the energy efficiency of PCM walls in office buildings located in various climatic regions in China for cooling. In the summer period, Lei et al. [28] have used the envelope heat gain reduction rate, which is a percentage reduction of the heat gains through the envelope due to the addition of PCM layer. In the work of Zwanzig et al. [29] PCM performance was evaluated according to three metrics: seasonal peak load shifting, seasonal peak load reduction, and total annual cooling and heating load reduction. Kuznik et al. [30], have experimentally investigated, in a full scale controlled test room, a PCM wall on a summer day, a winter day and a mid-season day. The results have shown that for all the cases tested, the decrement factor varies between 0.73 and 0.78. Mandilaras et al. [31] have presented the average monthly decrement factor and time lag values for a typical, two-storey, family house built in the mid-western part of Greece. Its walls consist of multiple layers of insulation materials and gypsum plasterboard panels containing PCMs. A decrease of the decrement factor by a further 30-40% and an increase on the time lag of approximately 100 min during late spring, early summer and autumn, attributed to the PCM implementation, are shown. Furthermore, in order to study the nonlinear behavior for PCM, the "mean-effective" specific heat capacity has been calculated. In [32] the authors have presented an experimental installation of real size,

concrete cubicles with PCM, constructed in the locality of Puigverd of Lleida (Spain), that can reduce the fluctuation of the external surface temperature of walls and obtain a time lag around + 2 h, compared to the base wall without PCM. In another investigation, by means of the use of PCM in the roof, numerically, Dong et al. have obtained a time delay of the temperature peak 3 hours higher than a common roof in the cold area of China [33]. In the experiment of Guarino et al. [34] a building-integrated thermal storage system in a cold climate has allowed solar radiation to be stored and released up to 6–8 hours. Thiele et al. [35] have evaluated the effects of adding PCM on the reduction and delay of thermal load through composite walls subjected to diurnal sinusoidal outdoor temperature and solar radiation heat flux.

The scientific literature analyzed highlights that there is not an existing general methodology for the evaluation of the dynamic characteristics of a PCM layer. Therefore, in this work the authors have elaborated a new procedure, based on a series of dynamic parameters evaluated in the monthly average day for every month through the year, which can be applied to any PCM type and location. The research was conducted in the laboratory of "Building Energy" of the Applied Physics Area of the Department of Mechanical, Energy and Management Engineering (DIMEG) at the University of Calabria. The aim of the work is to address the dynamic characterization of a PCM layer in which one or more bi-phase interfaces are formed, in the hypothesis that the thermal regime is a steady periodic regime. The boundary conditions of the layer are those which characterize the external walls of air-conditioned buildings. The analyses are developed as an explicit finite difference numerical model, which resolves the equation of conduction in solid phase and liquid phase and the equation of thermal balance at the bi-phase interfaces at the melting temperature. The temperature and heat flux trends on the external and internal surface, energy entering and exiting from the layer, and the stored energy in the layer in the sensible and latent form, are employed in order to define new parameters necessary to dynamically characterize the layer. Defined parameters are: latent storage efficiency; the fraction of latent energy stored compared to the total energy stored; decrement factor of the maximum excursion of the temperature and of the heat flux; the energy decrement factor; the time lag of the maximum and minimum peak of the temperature and heat flux; the fraction of the period during which the temperature and the heat flux maximum peak or minimum peak are constant in time on the internal surface. The procedure is used in order to evaluate dynamic characteristics of a PCM layer, with different melting temperatures and thermophysical characteristics. The climatic conditions taken into consideration, relating to two locations, one with a continental climate and the other one with a Mediterranean climate, are represented through the average monthly day and modeled with periodical non-sinusoidal fluctuations.

In a previous work [36] by the same authors, more complete examples of fields of temperature and of heat flux in the presence of one or more bi-phase interfaces, the evolution in time of the bi-

phase interface and the related trends of latent energies stored or released per unit time are described.

2. Methodology

2.1 Calculation model

The model constitutive equations are the general equation of thermal conductivity in the solid phase and in the liquid phase (1) and the balance equation at the bi-phase interface at the melting temperature (2) and (3):

$$\frac{\partial^2 T}{\partial x^2} - \frac{1}{a}\frac{\partial T}{\partial t} = 0 \quad (1) \qquad \left[k_l \frac{\partial T_l}{\partial x} - k_s \frac{\partial T_s}{\partial x}\right]_{x=X_M} = \rho H \frac{dX_M}{dt} \quad (2) \qquad T_l(X_M, t) = T_s(X_M, t) = T_M \quad (3)$$

With H representing latent heat of fusion, T_M melting temperature and X_M position of the bi-phase interface. Boundary conditions on the external surface of PCM layer are represented by the convective and radiative, at short and long wavelength, thermal exchanges with the outdoor environment, and on the internal surface by thermal exchanges with the indoor environment evaluated through the surface heat transfer coefficient. The corresponding equations are:

$$\Phi_e = \Phi_{r,e} + \Phi_{c,e} + \alpha\Phi_{sol} = h_{r,e}\left(T_{sky} - T_{s,e}\right) + h_{c,e}\left(T_{ea} - T_{s,e}\right) + \alpha\Phi_{sol} = -k\left.\frac{\partial T}{\partial x}\right|_{x=0} \quad (4)$$

$$\Phi_{ia} = h_{s,i}\left(T_{s,i} - T_{ia}\right) = -k\left.\frac{\partial T}{\partial x}\right|_{x=L} \quad (5)$$

with Φ_e signifying total heat flux from the outdoor environment, $\Phi_{r,e}$ longwave radiative heat flux exchanged with the sky, $\Phi_{c,e}$ convective heat flux exchanged with the external air, α_e absorption coefficient, Φ_{sol} solar radiation, $h_{r,e}$ and $h_{c,e}$ radiative and convective heat transfer coefficients, T_{sky} sky temperature, T_{ea} external air temperature, $T_{s,e}$ external surface temperature, Φ_{ia} heat flux transferred in the indoor environment, $h_{s,i}$ internal surface heat transfer coefficient, $T_{s,i}$ internal surface temperature, T_{ia} internal air temperature and L thickness of the layer.

An explicit finite difference numeric model has solved the equations system (1)-(5). The discretization of the equation, obtained by evaluating the time derivative with its related incremental ratio, leads to the relations for the calculation of the temperatures in the nodes not subject to a phase change and of the liquid fractions λ present in the subvolume of nodes at the melting temperature. Such equations and the employed calculation algorithm, validated by means of a comparison with the results determined by an analytical model that resolves the heat transfer in a PCM layer in a steady periodic regime [37], are reported in [36]. In detail, the algorithm provides for:

- the possibility that one or more bi-phase interfaces form in the layer, when the temperatures on the PCM boundary surfaces fluctuate around the melting temperature;
- a non-uniform spatial discretization;
- different thermo-physical properties in the solid phase and in the liquid phase;
- the update at every time instant of the resistances among nodes and of nodal heat capacities according to the position and typology of the bi-phase interfaces.

The model does not contemplate phenomena of phase segregation, of subcooling and of hysteresis. The position of the bi-phase interfaces is determined depending on the thickness and the liquid fractions λ_{j_k} present in sub volumes, with the relations:

$$X_{M,k} = \sum_{i=1}^{j_k-1} \Delta x_i + \Delta x_{j_k} \lambda_{j_k} \quad (6) \qquad X_{M,k} = \sum_{i=1}^{j_k-1} \Delta x_i + \Delta x_{j_k} (1 - \lambda_{j_k}) \quad (7)$$

In the previous equations, if the bi-phase interface is of melting (see Eq. 6), the position of the k-th bi-phase interface $X_{M,k}$ present in subvolume j_k is calculated summing the thicknesses of the subvolumes Δx_i preceding the node j_k to the portion of the subvolume j_k in liquid phase $\Delta x_{j_k} \lambda_{j_k}$. If it is a solidification interface (see Eq. 7), the position of the k-th bi-phase interface $X_{M,k}$ present in subvolume j_k is calculated summing the thicknesses of the subvolumes Δx_i preceding the node j_k to the portion of the subvolume j_k in solid phase $\Delta x_{j_k}(1 - \lambda_{j_k})$. For example, if the bi-phase interface is of melting and falls within the volume associated with the fourth node ($j_k = 4$), Eq. (6) provides $X_{M,k} = \Delta x_1 + \Delta x_2 + \Delta x_3 + \Delta x_4 \lambda_4$, with λ_4 fraction of volume 4 in liquid phase. Viceversa, if the bi-phase interface is of solidification, Eq. (7) provides $\Delta x_1 + \Delta x_2 + \Delta x_3 + \Delta x_4 (1 - \lambda_4)$, with $(1 - \lambda_4)$ fraction of volume 4 in solid phase.

All the equations and the algorithm have been implemented in our own MATLAB program code. Such a code allows us to determine the number and the position of eventual bi-phase interfaces in the layer, the phase configurations, the temperature and heat flux fields and the stored energy per unit time, the sum of latent and sensible contribution. In each point of the layer, the temperature and heat flux trends can be considered as the sum of a steady component and a fluctuating component. The steady component is calculated as an average of the instant values in the time period, and the fluctuating component is obtained by subtracting the steady component from the overall trend.

2.2 Phase configurations in the layer and surface temperatures and heat fluxes

Figures 1-4 show examples of temperature and heat flux trends on the layer external and internal surface. Such trends have been obtained considering the PCM S15, whose thermophysical properties are reported in Table 2 with reference to the boundary conditions, defined in Section 3, related to Turin. In order to be complete, the images also show the PCM melting temperature T_M,

the trends of the internal air temperature T_{ia} and also of the equivalent temperature of the outdoor environment $T_{e,eq}$ [17] which are representative of the three external loadings. In every image, the upper curves represent temperatures, whose scales are reported on the left axes, while the lower curves represent heat fluxes, whose scales are reported on the right axes. The vertical lines allow us to identify the time instants when the phase change process associated to each single bi-phase interface starts and ends, while the horizontal arrows indicate the duration of the phase change process associated with each single bi-phase interface. Figure 1 refers to the case of the absence of bi-phase interfaces and the layer is entirely in a solid phase (a) or in a liquid phase (b). Figure 2 shows the trends in the case of a bi-phase interface formation on the external surface (a) or on the internal surface (b). Figure 3 relates to the formation of two bi-phase interfaces, both on the external surface (a) or one on the internal surface and the other on the external surface (b). While, figure 4 relates to the case of the presence of three bi-phase interfaces all of them on the external surface (a) or two on the external surface and one on the internal surface (b).

Figure 1 – Absence of phase change a) solid phase b) liquid phase. Temperatures, $T_{s,e}$ and $T_{s,i}$, and heat fluxes, $\Phi_{s,e}$ and $\Phi_{s,i}$, on the external surface and on the internal surface; melting temperature T_M, internal air temperature T_{ia} and equivalent outdoor temperature $T_{e,eq}$.

Figure 2 – Presence of a bi-phase interface originating on the external surface a) or on the internal surface b). Temperatures, $T_{s,e}$ and $T_{s,i}$, and heat fluxes, $\Phi_{s,e}$ and $\Phi_{s,i}$, on the external surface and on the internal surface; melting temperature T_M, internal air temperature T_{ia} and equivalent outdoor temperature $T_{e,eq}$.

Figure 3 – Presence of two bi-phase interfaces both originating on the external surface a) or one on the external surface and the other on the internal surface b). Temperatures, $T_{s,e}$ and $T_{s,i}$, and heat fluxes, $\Phi_{s,e}$ and $\Phi_{s,i}$, on the external surface and on the internal surface; melting temperature T_M, internal air temperature T_{ia} and equivalent outdoor temperature $T_{e,eq}$.

Figure 4 – Presence of three bi-phase interfaces all originating on the external surface a) or two on the external surface and the other on the internal surface b). Temperatures, $T_{s,e}$ and $T_{s,i}$, and heat fluxes, $\Phi_{s,e}$ and $\Phi_{s,i}$, on the external surface and on the internal surface; melting temperature T_M, internal air temperature T_{ia} and equivalent outdoor temperature $T_{e,eq}$.

If the PCM layer is monophase, see figures 1a and 1b, the temperature in the entire layer is always higher than the melting temperature if the layer is in liquid phase, and is always lower than the melting temperature if the layer is in solid phase. The periodic temperatures and heat flux fluctuations on the internal surface present a lower amplitude and are shifted, compared to these on the external surface.

When the temperature on the external surface, see Figure 2, or on the internal surface of the layer, see Figure 2a, during the period, becomes equal to the melting temperature, a bi-phase interface forms. Such an interface penetrates the layer, it reaches maximum deepth, then it reverts direction and restores the initial monophase layer. Usually, during the winter season, at night time, the layer is totally in a solid phase; in the day time, due to the prevailing effect of solar radiation absorbed by the external surface and also due to the surface thermal exchange with the indoor environment, the layer heats up and the internal surface or the external surface reaches the melting temperature, starting the fusion process. The behavior is different during the months when the layer is entirely in a liquid phase in the day time. In fact, during nocturnal hours, due to the convective-radiative thermal exchange with the outdoor environment, the layer starts the solidification process. The interface penetrates the layer, and once a given deepth is reached, during daytime hours, it reverts direction mainly due to the absorbed solar radiation, and it restores the liquid phase in the whole layer. In both cases, during the phase change, the latent energy per unit time, proportional to the advancing speed of the bi-phase interface, at first increases, it reaches a certain maximum value and afterwards decreases until it is annulled at the instant when the bi-phase interface reverts direction and starts the opposite process. During this process, the latent energy per unit time always increases and it is at its maximum at the time instant when the phase change stops restoring the initial phase. Due to the effect of the velocity variation in the different time instants of the external loadings, the advancing velocity of the bi-phase interface is not constant in time. Because of this, the duration of the fusion process, which originates in the latent energy storage, is different from that of the solidification process, releasing the stored energy.

When the temperature on the external surface and on the internal surface of the layer become equal to the melting temperature, see Figure 3b, two bi-phase interfaces originated, and they can be both fusion interfaces if the initial layer is solid, or solidification interfaces if the initial layer is liquid. Both interfaces penetrate the layer, and reach a maximum deepth to finally be extinguished on the surface of origin. The two interfaces do not develop simultaneously and they both contribute to the latent energy storage and release process.

When the temperature on the external surface of the layer, in two successive time instants in the period, becomes equal to the melting temperature, two bi-phase interfaces originate on this surface, see Figure 3a. For instance, if the layer is totally in the liquid phase, the first bi-phase interface is a solidification one during nocturnal hours, and the other is a fusion one during diurnal hours, mainly produced by solar radiation. Such interfaces penetrate the layer at different velocities, and rejoin internally to re-establish the original monophase layer. The latent energy storage process is mainly connected to a bi-phase interface while the release process is connected to the other interface.

It can also happen that one of the two interfaces stays in the layer with a time length longer than the period P=24 hours, see Figure 4a, so that, in a defined interval of time in the period, three bi-

phase interfaces are present in the layer. Also in this case, the latent energy stored by one interface is completely returned by the other one. It is also possible that, in the case when three bi-phase interfaces are present, two originate on the external surface, while a third one is always present in period P and fluctuates concerning a portion of the layer near to the internal surface, see figure 4b. Also in this case, the two interfaces originating on the external face, rejoin in the inner part of the layer and the stored latent energy is completely returned by the other one. The energy stored by the third interface is then released by the same one with a similar trend.

The phase change effects within the layer on the surface temperature and heat flux trends can be summarized as follows. Regarding the temperature trend on the surface where the bi-phase interfaces originate, see Figures 2 and 3, unlike a monophase material, it is revealed that:

a) for a fraction of the period the related maximum or minimum peaks are constant and approximate to the melting temperature;
b) the maximum or the minimum peak persists in time;
c) the maximum excursion in the period is reduced due to decrement of the maximum peak amplitude, if the interface is one of fusion, or that of the minimum peak, if the interface is one of solidification;

Concerning the heat flux trend:

- if the bi-phase interfaces originate on the external surface, on this surface it is highlighted that:
  d) at the beginning and at the end of the phase change there is discontinuity;
  e) the daily maximum excursion increases;
  f) the instant when the maximum or the minimum peak occur changes;
  g) the fluctuant energy changes.
- if the bi-phase interfaces originate on the internal surface, on this surface it is noticed that:
  h) at the beginning and at the end of the phase change there is a discontinuity;
  i) for a fraction of the period, the related maximum or minimum peak can be considered constant;
  j) the daily maximum excursion decreases;
  k) the instant when the maximum or the minimum peak occur changes;
  l) the fluctuant energy decreases.

On the surface that is not the site of bi-phase interface formation, if it is the internal one, the maximum excursions decrease and the fluctuating temperature and heat flux maximum and minimum peaks undergo a time lag. Whereas, if it is the external one, the fluctuations of temperature and heat flux stay basically unchanged. Furthermore, increasing the number of the bi-phase interfaces on the external surface, the thermal fluctuations on the internal surface result as being damped until a complete attenuation with three bi-phase interfaces is reached, see Figure 4a. Finally, the contemporary presence of bi-phase interfaces on the internal and external surfaces, see

Figures 3b and 4b, causes analogous behavior on the external surfaces to those described in the previous a) - g) points, while on the internal surface the maximum temperature and heat flux excursions are almost completely damped. The above described trends show that, for the complete dynamic characterization of the PCM layer, the employment of more parameters is necessary, as defined in section 2.4, in order to identify fully the transformation that the form of the fluctuating thermal quantity undergoes when passing through the layer.

2.3 Fluctuating transferred energy and latent and total stored energy

The monthly average daily fluctuant energy on the internal surface $\widetilde{E}_i$ and external surface $\widetilde{E}_e$ of the layer are calculated taking into account that, for a fluctuating quantity around a mean value, the area subtended the trend in the time interval in which the quantity is greater than the average value is equal to the area subtended the trend in the time interval in which the quantity is less than the average value. For this reason, $\widetilde{E}_i$ e $\widetilde{E}_e$ are determined by half of the numeric integral in time, extended to the period, of the absolute value of the surface fluctuant heat fluxes $\widetilde{\phi}_{s,i}$ and $\widetilde{\phi}_{s,e}$ (Eqs. 8 - 9).

$$\widetilde{E}_i = \frac{1}{2}\sum_{n=0}^{P}\left|\widetilde{\phi}_{s,i}\right|\Delta t \qquad (8) \qquad \widetilde{E}_e = \frac{1}{2}\sum_{n=0}^{P}\left|\widetilde{\phi}_{s,e}\right|\Delta t \qquad (9)$$

The total energy stored E_T is calculated by half of the numeric integral in time, extended to the period, of the difference, in absolute value, of the heat flux entering the layer and exiting from the layer (Eq. 10). Likewise, the advancing velocity of the bi-phase interface k, given by the ratio $(X_{M,k}^{n+1} - X_{M.k}^{n})/\Delta t$, is used to evaluate the latent energy stored, by the Eq. (11).

$$E_T = \frac{1}{2}\sum_{n=0}^{P}|\phi_T|\Delta t = \frac{1}{2}\sum_{n=0}^{P}\left|\phi_{s,i} - \phi_{s,e}\right|\Delta t \quad (10) \qquad E_L = \frac{1}{2}\sum_{n=0}^{P}|\phi_L|\Delta t = \frac{1}{2}\sum_{n=0}^{P}\left|\rho H\frac{\left(X_{M,k}^{n+1} - X_{M.k}^{n}\right)}{\Delta t}\right|\Delta t \quad (11)$$

2.4 Definition of the dynamic parameters

With reference to a period P=24 hours, the temperature and heat flux trends on the external surface and on the internal surface, the fluctuant energy entering in the layer $\widetilde{E}_e$ and exiting from the layer $\widetilde{E}_i$, and the stored energy in the form of latent energy E_L, are used in order to define the parameters necessary to dynamically characterize the PCM layer.

Figure 5 – Representation of the thermal quantities used for the definition of the dynamic parameters of the PCM layer. a) temperature trends on the external surface $T_{s,e}$ and on the internal surface $T_{s,i}$; b) heat flux trend on the external

surface $\Phi_{s,e}$ and on the internal surface $\Phi_{s,i}$; c) fluctuating energy on the external surface $\tilde{E}_e$ and on the internal surface $\tilde{E}_i$; d) sensible E_S, latent E_L and total E_T energy stored.

With reference to Figure 5, such parameters are:

a) the latent storage efficiency ε_L, ratio between the latent energy stored E_L and the maximum storable $E_{L,max}$ latent energy, evaluated on the basis of the assumption that the whole layer changes phase; the fraction of latent energy $\Lambda_L$with respect to total energy stored in the layer, see Figure 5d:

$$\varepsilon_L = \frac{E_L}{E_{L,max}} = \frac{\rho H \Delta x_{PC}}{\rho H L} \qquad (12) \qquad\qquad \Lambda_L = \frac{E_L}{E_T} \qquad (13)$$

b) the decrement factor of the maximum excursion of the temperature f_T (Eq. 14), see figure 5a, and of the heat flux f_Φ (Eq. 15), see Figure 5b, and the decrement factor of the fluctuating energy transferred f_E (Eq. 16), see Figure 5c:

$$f_T = \frac{T_i^{max} - T_i^{min}}{T_e^{max} - T_e^{min}} \qquad (14) \qquad f_\Phi = \frac{\Phi_i^{max} - \Phi_i^{min}}{\Phi_e^{max} - \Phi_e^{min}} \qquad (15) \qquad f_E = \frac{\widetilde{E}_i}{\widetilde{E}_e} \qquad (16)$$

c) the time lag of the maximum and the minimum peak of the temperature $\Delta t_{T^{max}}$ and $\Delta t_{T^{min}}$ (Eqs. 17-18), see Figure 5a, and of the heat flux $\Delta t_{\Phi^{max}}$ and $\Delta t_{\Phi^{min}}$ (Eqs. 19-20), see Figure 5b:

$$\Delta t_{T^{max}} = \left(t_{T_i^{max}} - t_{T_e^{max}}\right) \qquad (17) \qquad \Delta t_{T^{min}} = \left(t_{T_i^{min}} - t_{T_e^{min}}\right) \qquad (18)$$

$$\Delta t_{\Phi^{max}} = \left(t_{\Phi_i^{max}} - t_{\Phi_e^{max}}\right) \qquad (19) \qquad \Delta t_{\Phi^{min}} = \left(t_{\Phi_i^{min}} - t_{\Phi_e^{min}}\right) \qquad (20)$$

d) the constant peak time fraction of the temperature or of the heat flux, namely the fraction of period P in which the maximum or the minimum peak Π_{T_i} (Eq. 21), see Figure 5a, and of heat flux Π_{Φ_i} (Eq. 22), see figure 5b, on the internal surface are constant.

$$\Pi_{T_i} = \frac{\Delta P_{T_i^p = const}}{P} \qquad (21) \qquad\qquad \Pi_{\Phi_i} = \frac{\Delta P_{\Phi_i^p = const}}{P} \qquad (22)$$

In the previous equations, the subscripts *i* and *e* indicate respectively the internal and external surface of the layer, while the superscripts *p*, *max* and *min* identify the generic peak value, the

maximum value and minimum value of the considered thermal quantity. If the parameter Π is different to zero, for the evaluation of the time lag (Eqs. 17-20), the time *t* to be considered is that at the beginning of the fraction of the period in which the maximum or minimum peak of the thermal quantity is constant, see Figures 5a and 5b.

The defined dynamic parameters allow us to quantify the decrement and the time lag which temperature and heat flux fluctuations undergo when passing through the layer and the extent of the latent thermal storage in the layer. All the parameters defined are to be used either in the absence of or in the presence of phase change. In Table 1 some special cases of combinations of the parameters are reported and for each case an indication to thermally size the layer well. In the absence of phase change Π_{T_i}, Π_{Φ_i}, ε_L and Λ_L are nil and the dynamic parameters are reduced to those characteristics of a monophase layer. In the presence of phase change, parameters Π_{T_i}, Π_{Φ_i}, ε_L and Λ_L identify the behavior of the layer both in energetic terms and as damping of thermal fluctuations. In fact, from the analysis of Eqs. (12), (13), (21) and (22), with an increase of Π_{T_i} and Π_{Φ_i} the fraction of the period in which the thermal fluctuations on the internal surface are completely damped increases, while with a growth of ε_L and Λ_L, the portion of the layer interested by the phase change and the fraction of latent energy stored compared to sensible one, respectively, increase.

Table 1 - Description of the dynamic behavior of a PCM layer in some special cases and related latent storage parameter values, ε_L and Λ_L and of the constant peak time fractions Π_{T_i} and Π_{Φ_i}.

3 Case study description

The calculation procedure for the determination of the thermal fields and of the stored energy was used in order to evaluate, on a monthly basis, the energetic and dynamic characteristics of five different PCM typologies (see Table 2), all of a thickness equal to 6 cm. Melting temperatures, ranging from 15°C to 32°C, were chosen in relation to the set point temperatures of air-conditioned environments in summer and winter periods. In the analysis, two locations with quite different climatic conditions, Turin (TO) and Cosenza (CS) were considered. The solar irradiation on the horizontal plane G and external air temperature T_{ea} data employed, relative to the monthly average days of a whole year, are those from the national standard reference [38] and are shown in Table 3, respectively, in the first and in the second row for each location. The typical day of each month, represented through the monthly average hourly values of solar radiation on the vertical plane exposed to South, of the sky temperature and of external air temperature, were generated starting from monthly average daily values using TRNSYS 17 [39] software. In the indoor environment, the temperature values in continuous regime were chosen according to the reference standard [40] while the heating period, the cooling period and the intermediate period according to the national regulations [41], see Table 4. The numerical simulations considered: on the external surface a solar

absorption coefficient equal to 0.60 and a convective and radiative heat transfer coefficient respectively equal to 20 W/m^2 K and 5.35 W/m^2 K; on the internal surface a heat transfer coefficient equal to 7.7 W/m^2. The heat transfer coefficients were taken from the EN ISO 6946 [42] standard and from a previous experimental work by the authors [43]. The layer was discretized with 19 nodes and the equation system was solved by an integration step Δt=5 seconds. The choice of the number of nodes was performed by preliminary simulations in order to verify the grid independence. From the results of the simulations performed, varying the number of nodes from 10 to 30 with a step of one, it is possible to deduce that this condition is realized by using nineteen nodes to discretize the PCM layer.

Table 2 – Thermophysical properties of the different types of PCMs.

Table 3 - Monthly average daily values of a whole year of the external air temperature T_{ea} and solar irradiation on the horizontal plane G in Turin and Cosenza.

Table 4 - Indoor environment set point temperature in the different months for Turin and Cosenza.

4 Results and discussion

4.1 Phase configuration in the different typologies of PCM layers

Figures 6 and 7 show the number of bi-phase interfaces, the surface on which they originate and the disposition of the phases in the layer starting from the outside and going towards the inside, for the considered PCMs and locations in the different months. The presence of a bi-phase interface which originates on the external surface is indicated by 1a), and that which originates on the internal surface by 1b). The case of two bi-phase interfaces, both originating on the external surface, is shown by 2a), while the case with one interface on the external surface and another on the internal surface by 2b); Finally, in the case of three bi-phase interfaces, 3a) shows that all the interfaces originate on the external surface, while 3b) shows that two interfaces are formed on the external surface and the other one on the internal surface.

Figure 6 - Number of interfaces present in the layer, surface on which they originate, and arrangement of the phases from the outside to the inside, in the various months of the year and for different PCMs. Turin. a) all the bi-phase interfaces are on the external surface; b) one bi-phase interface is on the internal surface.

Figure 7 - Number of interfaces present in the layer, surface on which they originate, and arrangement of the phases from the outside to the inside in the various months of the year and for different PCMs. Cosenza. a) all the bi-phase interfaces are on the external surface; b) one bi-phase interface is on the internal surface.

The phase changes occur: for PCM S15 from September to May, except in January, in Turin, and from October to May in Cosenza; for PCM LATEST20T from April to October in Turin, and from February to December in Cosenza; for PCM HS22P from May to September in Turin, and from April to November in Cosenza; for PCM SP26E from June to September in Turin, and from May to November in Cosenza; the PCM C32, due to the high melting temperature, in Turin does not undergo any phase change, while in Cosenza phase changes occur from July to September.

4.2 Monthly values of dynamic parameters

In Figure 8 values of dynamic parameters Λ_L, ε_L, f_T, f_Φ and f_E are shown in the different months, calculated by Eqs. 12-16.

Figure 8 - Stored latent energy fraction in the layer Λ_L, latent stored efficiency ε_L and decrement factors f_T, f_Φ and f_E, during the different months for Turin, on the left, and for Cosenza, on the right.

The fraction of stored latent energy in layer Λ_L shows in the months in which, the latent storage is prevalent over the sensible one. The latent storage efficiency ε_L shows in which months the part of the layer interested by the phase change is more extended. The decrement factor of the maximum excursion of the temperature f_T in the presence of phase changes it reduces and, in the months with the highest stored latent energy, is annulled. The decrement factor of the maximum excursion of the heat flux f_Φ and the decrement factor of the energy f_E exhibit similar trends and values, and in the presence of a phase change present analogous behavior of f_T.

In the fraction of the period in which the maximum or minimum peak of the temperature on the internal surface is constant, also the related heat flux peak is constant, due to the fact that the indoor environment temperature is fixed and equal to the set-point value. For this reason, in air-conditioned situations $\Pi_{T_i} = \Pi_{\Phi_i}$. With reference to all considered cases, only for PCMs S15 and LATEST20T, and for both locations, it can be observed that, in some months the maximum and minimum peaks of the temperature and heat flux, stay constant for a fraction of the period. For these PCMs the values of the parameter $\Pi_{T_i} = \Pi_{\Phi_i}$ are shown in Table 5.

Table 5 - Constant peak time fraction $\Pi_{T_i} = \Pi_{\Phi_i}$ during the different months for Turin and Cosenza.

The constant peak time fraction is different to zero during the months when a bi-phase interface originates on the internal surface, or when a bi-phase interface fluctuates within the layer, close to the internal surface. This can be seen from the comparison between Table 5 and Figures 6 and 7. In those figures, this case is indicated by the letter b, independently from the number of bi-phase interfaces in the layer.

In Figure 9 the values of time lags $\Delta t_{T^{max}}$, $\Delta t_{T^{min}}$, $\Delta t_{\Phi^{max}}$ and $\Delta t_{\Phi^{min}}$ are shown in the different months, calculated by Eqs. 17-20. In absence of phase change, they are almost constant, with the exception of that of the minimum peak of the heat flux, which shows a seasonal variability; in the presence of one or more bi-phase interfaces the time lags are subject to abrupt variations. In particular, in the absence of phase change, for both locations considered and for all the different PCMs, with the change of the months, the $\Delta t_{T^{max}}$ and $\Delta t_{T^{min}}$ variation field is within 0 and 3 hours, while that of $\Delta t_{\Phi^{max}}$ is between 2.5 and 6 hours. The time lag $\Delta t_{\Phi^{min}}$ varies between 5 and 7 hours in the summer period and between 13 and 16 hours in the winter period. In the presence of phase change, the extent of variations is the function of the PCM, of the locality and of the month.

Figure 9 – Time lags of temperature peaks $\Delta t_{T^{max}}$ and $\Delta t_{T^{min}}$, and of heat flux peaks $\Delta t_{\Phi^{max}}$ and $\Delta t_{\phi^{min}}$, in different months, for Turin on the left, and for Cosenza on the right.

4.3 Influence of the latent storage efficiency on the dynamic characteristics

Data analysis has shown that the dynamic parameters related to the trends of the temperature and heat flux, of the fluctuating energy passing through the layer and of the stored energy in latent and sensible form are correlated to the latent storage efficiency. Figure 10 shows the values of dynamic parameters related to the monthly average day of the latent energy fraction Λ_L, and the decrement factors f_T, f_Φ and f_E depending on the latent storage efficiency ε_L. In each image the values related to both locations and for the different PCMs are reported.

Figure 10 – Latent energy fraction stored Λ_L and decrement factor of temperature f_T, of heat flux f_Φ and of the energy f_E in function of the latent storage efficiency ε_L, related to both locations and for the different PCMs.

Generally, irrespective of location, of PCM typology and of the air-conditioning season, to the increase of latent storage efficiency ε_L, the decrement factors of the maximum excursion of the temperature f_T and of the heat flux f_Φ as well as the decrement factor of the energy decrease, while the stored latent energy fraction Λ_L rises significantly. All these trends can be represented by second grade polynomial functions, with concavity facing downwards for parameters Λ_L and f_T, and facing upwards for parameters f_Φ and f_E. Concerning the decrement factor of the temperature f_T trend, it is necessary to specify that, during the months when the constant peak time fraction is different to zero, it is subject to a change of concavity with a reduction of the values. This different behavior is recorded by the image with two interpolating curves with opposite concavities (conf. *a* and conf. *b*). Regarding the other dynamic parameters, the influence of the constant peak time fraction is very contained and the trends can be considered independent to the configuration of the phases within the layer.

In general, the image concerning the latent energy fraction Λ_L shows a strict correlation to the latent storage efficiency ε_L and it is an indicator that the total stored energy apportionment in latent and sensible energy depends mainly on the latent storage efficiency ε_L. Concerning the decrement factors f_T, f_Φ and f_E, the images highlight that for reduced ε_L values, to which corresponds a greater contribution of the sensible type to the thermal storage, the dispersion of the points around the interpolating curves is greater, due to the different volumetric heat capacity ρc_p in the different PCMs. For higher values of ε_L, to which corresponds a contribution to the heat storage in latent form prevailing on the sensible one, the points show a lower dispersion. Furthermore, images show that it is sufficient to obtain a latent storage efficiency $\varepsilon_L = 0.35$, to which corresponds a portion of the layer involved in the phase change equal to 35%, in order to attenuate completely the maximum excursion of the temperature and heat flux on the internal surface, to annul the fluctuating energy transferred into the indoor environment and to obtain unitary values of the latent energy fraction.

Similarly to Figure 10, in Figure 11, the values of the time lag of maximum peak and of the minimum peak of the temperature Δt_T^{max} and Δt_T^{min} and of the heat flux Δt_ϕ^{max} and Δt_ϕ^{min} as a function of the latent storage efficiency ε_L are reported.

Figure 11 - Time lag of the maximum and minimum peak of the temperature Δt_T^{max} and Δt_T^{min} and of the heat flux Δt_ϕ^{max} and Δt_ϕ^{min} as a function of latent storage efficiency ε_L, related to both locations and for the different PCMs.

On the whole, independently from the location, PCM type, and air-conditioning season, with the rise of latent storage efficiency ε_L, time lags Δt_T^{max}, Δt_T^{min} and Δt_ϕ^{max} increase. Such an increase is more contained for the time lag Δt_T^{min}. Concerning the time lag Δt_ϕ^{min}, functional dependency on the growth of ε_L, is different in the two air-conditioning seasons, with a reduction in the winter period and an increase in the summer period. For such a reason, in the image relative to time lag Δt_ϕ^{min}, the pointers were differentiated based on the air-conditioning season. All these trends can be represented by a first or second grade polynomial function. The time lags of the temperature maximum and minimum peak, analogously to the temperature decrement factor, are distant from the interpolating straight line during the months when the constant peak time fraction is different to zero. For the other parameters, the influence of the constant peak time fraction is very contained and the trends can be considered independent from the configuration of the phases in the layer. Furthermore, the summary shown in the image in Figure 11, highlights that the functional dependency between the dynamic parameters and the latent storage efficiency provides a qualitative trend with a high dispersion. The interpolating curves show that with a storage latent efficiency $\varepsilon_L = 0.35$, the time lag of the maximum peak of the temperature and of the heat flux increase by about 10 hours, the time lag of the minimum peak of the temperature rises by about 5 hours, and the time lag

of the minimum peak of the heat flux decreases by about 6 hours during the winter period, and increases by about 5 hours in the summer period.

4.4 Correlations between dynamic parameters

A further study has been developed by correlating dynamic parameters directly among them. The search of such functional links highlighted a strong correlation between the decrement factor of the heat flux maximum excursion f_Φ and the decrement factor of the energy f_E, and between the time lag of the maximum peak of the temperature Δt_T^{max} and the time lag of the maximum peak of the heat flux Δt_Φ^{max}. Such dependencies, see Figure 12, result as being independent of the location, of the typology of PCM, of the configuration of the phases in the layer, and of the air-conditioning season.

Figure 12 – Energy decrement factor in function of that of the heat flux f_ϕ, on the left, and heat flux maximum peak time lag Δt_Φ^{max} in function to the temperature maximum peak time lag Δt_T^{max}.

The decrement factor f_E increases linearly with a growth of the decrement factor f_Φ with an angular coefficient close to the unit and, in these conditions, the intercept at the origin represents the difference between the two dynamic parameters, for all the values of f_Φ, see Eq. (24). Analogously it happens for the time lags Δt_Φ^{max} and Δt_T^{max}, see Eq. (25). In both cases, the positive value of the intercept at the origin shows that f_E and Δt_Φ^{max} are, respectively, higher than f_Φ and Δt_T^{max}.

4.5 Parameters required for the dynamic characterization

The analysis developed in the previous sections of this work shows that, for the complete characterization of a PCM layer subject to a phase change, it is necessary to evaluate only a part of the parameters as defined in Section 2.4. These parameters are: the decrement factor of the temperature f_T and heat flux f_Φ maximum excursion; the temperature maximum and minimum peak time lag Δt_T^{max} and Δt_T^{min}; the heat flux minimum peak time lag Δt_Φ^{min}; the latent storage efficiency ε_L; the constant peak time fraction of the internal surface temperature and heat flux Π_{T_i} and Π_{Φ_i}. The other parameters can be calculated with a high level of accuracy by Eq. 23 for the fraction of the latent energy stored Λ_L, by Eq. 24 for the energy decrement factor f_E and by Eq. 25 for the heat flux maximum peak time lag Δt_Φ^{max}.

$$\Lambda_L = -8.0177\,\varepsilon_L^2 + 5.5839\,\varepsilon_L + 0.0074 \tag{23}$$

$$f_E = 0.9783\,f_\phi + 0.0243 \tag{24}$$

$$\Delta t_\Phi^{max} = 0.916\,\Delta t_T^{max} + 2.4047 \tag{25}$$

In the end, in a situation of continuous air-conditioning, since $\Pi_{T_i} = \Pi_{\Phi_i}$, the number of dynamic parameters required in order to identify in a complete way the dynamic behavior of the layer decreases from eleven to seven. Moreover, with less accuracy, also the decrement factor of the heat flux maximum excursion f_ϕ can be correlated to the latent storage efficiency by the relation:

$$f_\phi = 2.9719\,\varepsilon_L^2 - 1.8166\,\varepsilon_L + 0.2979 \qquad (26)$$

5. Conclusions

In this work, an accurate thermal analysis of PCM layers subject to the typical loadings operating on the external walls of air-conditioned buildings has been developed in the case in which, due to the effect of the periodic boundary conditions one or more bi-phase interfaces are present in the layer. The analysis allowed for the evaluation of the effects produced by the phase change on the heat transfer of the temperature and heat flux fluctuations, and on the thermal storage within the layer.

For a complete dynamic characterization of the PCM layer, it was necessary to define more parameters in order to identify the change that undergoes the form of the trend of temperature and heat flux, as well as the transferred fluctuating energy and the sensible and latent energy stored. Concerning the temperature fluctuation, the decrement factor of the maximum excursion, the maximum and minimum peak time lag and the constant peak time fraction on the internal surface have to be used in order to quantify the thermal discomfort following the variation of the internal surface temperature, both during the winter and summer season. If the heat flux is considered, the analogue parameters provide the extent of the attenuation and of the time lag of the power peak, entering during the summer and exiting in the winter, for the evaluation of the maximum loads which work on the indoor environment. Furthermore, if the fluctuating energy passing through the layer is considered, the relative decrement factor allows estimation of the fraction of transferred energy into the indoor environment in summer and winter air-conditioning, for the determination of the thermal requirements. Finally, the latent storage efficiency and the fraction of stored latent energy Λ_L allow evaluation of the correct use of the layer as a system of latent heat storage. The defined parameters have to be utilized for the thermal dimensioning of the layer, which is related to the choice of PCM and to its thickness, and also to identify the thermal behavior of the layer when operating.

Variability of the configurations of the phases in the layer during the course of the year modify the dynamic characteristics of the layer in function to the quantity of the latent energy stored. In particular, it has been found that the dynamic parameters are correlated to the latent storage efficiency. The latent storage fraction and the decrement factors are strongly correlated, while for

the time lags the correlation is less accurate. Independently from the location, from the type of PCM and from the configuration of the phases in the layer, by increasing the latent storage efficiency:

- the maximum excursion decrement factor of the temperature and the heat flux, and the decrement factor of the energy decrease;
- the latent energy fraction stored increases drastically;
- the maximum and minimum peak time lags of temperature and the maximum peak time lag of heat flux increase;
- the minimum peak time lag of heat flux decreases in the winter season and increases in the summer season;

Finally, results show that it is sufficient to reach the phase change in a portion of the layer equal to 35% in order to obtain:

- a complete attenuation on the internal surface of the temperature and heat flux maximum excursion;
- an annulment of the fluctuating energy transferred to the indoor environment;
- unitary values of the latent energy fraction;
- a high increase of the time lag of the maximum and minimum peak of temperature, of the maximum peak of the heat flux, of the minimum peak of the heat flux during summer period;
- a high reduction of the minimum peak of the heat flux during the winter period.

The research of further functional dependencies among the dynamic characteristics highlighted a strong correlation between the decrement factor of the maximum excursion of the heat flux and the energy decrement factor, and between the time lag of the maximum peak of the temperature and the time lag of the maximum peak of the heat flux. Finally, it can be concluded that in order to identify the PCM layer's dynamic behavior in a complete way, seven independent dynamic parameters are necessary, from which it is possible to obtain the remaining parameters.

Nomenclature

a	thermal diffusivity [m^2/s]
c	specific heat capacity [J/kg K]
E	energy per square meter [J/m^2]
E_e	energy on the external surface [J/m^2]
E_i	energy on the internal surface [J/m^2]
f_T	decrement factor of the temperature maximum excursion [-]
f_Φ	decrement factor of the heat flux maximum excursion [-]
f_E	decrement factor of the fluctuating energy transferred [-]
G	monthly average daily solar irradiation on the horizontal plane [J/m^2]
h	heat transfer coefficient [$W/(m^2 K)$]

H	latent heat of fusion [J/kg]
j_k	j-th subvolume including the k-th bi-phase interface [-]
k	thermal conductivity [W/m K]
L	layer thickness [m]
P	period [s]
t	time [s]
T	Temperature [K]
x	spatial coordinate [m]
X_M	position of the bi-phase interface [m]
Greek symbols	
α	solar absorption coefficient [-]
ΔP	portion of period P [h]
Δt	finite difference time step [s]
$\Delta t_{T^{max}}$	time lag of the temperature maximum peak [h]
$\Delta t_{T^{min}}$	time lag of the temperature minimum peak [h]
$\Delta t_{\Phi^{max}}$	time lag of the heat flux maximum peak [h]
$\Delta t_{\Phi^{min}}$	time lag of the heat flux minimum peak [h]
Δx	thickness of the subvolume [m]
ε_L	latent energy efficiency [-]
Φ	heat flux [W/m^2]
λ	liquid fraction [-]
Λ_L	latent energy fraction [-]
Π_{T_i}	constant peak time fraction of the temperature
Π_{Φ_i}	constant peak time fraction of the heat flux
ρ	density [kg/m^3]
Subscripts	
c	convective
e	external
eq	equivalent
ea	referring to the external air load
i	i-th subvolume preceeding the subvolume in phase change
ia	internal air
j_k	referring to the j-th subvolume including the k-th bi-phase interface
k	k-th bi-phase interface
l	liquid
L	referring to the latent energy stored
L,max	referring to the maximum latent energy stored
M	melting
n	n-th hour
p	at constant pressure
PC	phase change

r	radiative
s	solid
S	referring to the sensible energy stored
s,i	referring to the internal surface
s,e	referring to the external surface
sky	referring to the sky load
sol	referring to the solar load
T	referring to the total energy stored
Superscripts	
max	maximum value
min	minimum value
n	current time instant
n+1	successive time instant
p	peak value
sum	summer period
win	winter period
Symbols	
~	fluctuating value

References

[1] Hussein Akeiber, Payam Nejat, Muhd Zaimi Abd. Majid, Mazlan A. Wahid, Fatemeh Jomehzadeh, Iman Zeynali Famileh, John Kaiser Calautit, Ben Richard Hughes, Sheikh Ahmad Zaki, A review on phase change material (PCM) for sustainable passive cooling in building envelopes, Renewable and Sustainable Energy Reviews, Volume 60, July 2016, Pages 1470-1497.

[2] Yinping Zhang, Guobing Zhou, Kunping Lin, Qunli Zhang, Hongfa Di, Application of latent heat thermal energy storage in buildings: State-of-the-art and outlook, Building and Environment, Volume 42, Issue 6, June 2007, Pages 2197-2209, ISSN 0360-1323, http://dx.doi.org/10.1016/j.buildenv.2006.07.023.

[3] Frédéric Kuznik, Damien David, Kevyn Johannes, Jean-Jacques Roux, A review on phase change materials integrated in building walls, Renewable and Sustainable Energy Reviews, Volume 15, Issue 1, January 2011, Pages 379-391, ISSN 1364-0321, http://dx.doi.org/10.1016/j.rser.2010.08.019.

[4] Mario A. Medina, Jennifer B. King, Meng Zhang, On the heat transfer rate reduction of structural insulated panels (SIPs) outfitted with phase change materials (PCMs), Energy, Volume 33, Issue 4, April 2008, Pages 667-678, ISSN 0360-5442, http://dx.doi.org/10.1016/j.energy.2007.11.003.

[5] Amar M. Khudhair, Mohammed M. Farid, A review on energy conservation in building applications with thermal storage by latent heat using phase change materials, Energy Conversion and Management, Volume 45, Issue 2, January 2004, Pages 263-275, ISSN 0196-8904, http://dx.doi.org/10.1016/S0196-8904(03)00131-6.

[6] L.F. Cabeza, A. Castell, C. Barreneche, A. de Gracia, A.I. Fernández, Materials used as PCM in thermal energy storage in buildings: A review, Renewable and Sustainable Energy Reviews, Volume 15, Issue 3, April 2011, Pages 1675-1695, ISSN 1364-0321, http://dx.doi.org/10.1016/j.rser.2010.11.018.

[7] Belén Zalba, José M Marín, Luisa F. Cabeza, Harald Mehling, Review on thermal energy storage with phase change: materials, heat transfer analysis and applications, Applied Thermal Engineering, Volume 23, Issue 3, February 2003, Pages 251-283, ISSN 1359-4311, http://dx.doi.org/10.1016/S1359-4311(02)00192-8.

[8] Vineet Veer Tyagi, D. Buddhi, PCM thermal storage in buildings: A state of art, Renewable and Sustainable Energy Reviews, Volume 11, Issue 6, August 2007, Pages 1146-1166, ISSN 1364-0321, http://dx.doi.org/10.1016/j.rser.2005.10.002.

[9] Ruben Baetens, Bjørn Petter Jelle, Arild Gustavsen, Phase change materials for building applications: A state-of-the-art review, Energy and Buildings, Volume 42, Issue 9, September 2010, Pages 1361-1368, ISSN 0378-7788, http://dx.doi.org/10.1016/j.enbuild.2010.03.026.

[10] Michal Pomianowski, Per Heiselberg, Yinping Zhang, Review of thermal energy storage technologies based on PCM application in buildings, Energy and Buildings, Volume 67, December 2013, Pages 56-69, ISSN 0378-7788, http://dx.doi.org/10.1016/j.enbuild.2013.08.006.

[11] N. Soares, J.J. Costa, A.R. Gaspar, P. Santos, Review of passive PCM latent heat thermal energy storage systems towards buildings' energy efficiency, Energy and Buildings, Volume 59, April 2013, Pages 82-103, ISSN 0378-7788, http://dx.doi.org/10.1016/j.enbuild.2012.12.042.

[12] Hicham Johra, Per Heiselberg, Influence of internal thermal mass on the indoor thermal dynamics and integration of phase change materials in furniture for building energy storage: A review, Renewable and Sustainable Energy Reviews, Volume 69, March 2017, Pages 19-32, ISSN 1364-0321, http://dx.doi.org/10.1016/j.rser.2016.11.145.

[13] Mohammad Saffari, Alvaro de Gracia, Svetlana Ushak, Luisa F. Cabeza, Economic impact of integrating PCM as passive system in buildings using Fanger comfort model, Energy and Buildings, Volume 112, 15 January 2016, Pages 159-172, ISSN 0378-7788, http://dx.doi.org/10.1016/j.enbuild.2015.12.006.

[14] EN ISO 13786, Thermal Performance of Buildings Components e Dynamic Thermal Characteristics e Calculation Methods, 2010.

[15] G. Evola, L. Marletta, A dynamic parameter to describe the thermal response of buildings to radiant heat gains, Energy and Buildings, Volume 65, October 2013, Pages 448-457, ISSN 0378-7788, http://dx.doi.org/10.1016/j.enbuild.2013.06.026.

[16] G. Oliveti, N. Arcuri, D. Mazzeo, M. De Simone, A new parameter for the dynamic analysis of building walls using the harmonic method, International Journal of Thermal Sciences, Volume 88, February 2015, Pages 96-109, ISSN 1290-0729, http://dx.doi.org/10.1016/j.ijthermalsci.2014.09.006.

[17] D. Mazzeo, G. Oliveti, N. Arcuri, Influence of internal and external boundary conditions on the decrement factor and time lag heat flux of building walls in steady periodic regime, Applied Energy, Volume 164, 15 February 2016, Pages 509-531, ISSN 0306-2619, http://dx.doi.org/10.1016/j.apenergy.2015.11.076.

[18] D. Mazzeo, G. Oliveti, N. Arcuri, Mapping of the seasonal dynamic properties of building walls in actual periodic conditions and effects produced by solar radiation incident on the outer and inner surfaces of the wall, Applied Thermal Engineering, Volume 102, 5 June 2016, Pages 1157-1174, ISSN 1359-4311, http://dx.doi.org/10.1016/j.applthermaleng.2016.04.039.

[19] K.J. Kontoleon, D.K. Bikas, The effect of south wall's outdoor absorption coefficient on time lag, decrement factor and temperature variations, Energy and Buildings, Volume 39, Issue 9, September 2007, Pages 1011-1018, ISSN 0378-7788, http://dx.doi.org/10.1016/j.enbuild.2006.11.006.

[20] Andrea Gasparella, Giovanni Pernigotto, Marco Baratieri, Paolo Baggio, Thermal dynamic transfer properties of the opaque envelope: Analytical and numerical tools for the assessment of the response to summer outdoor conditions, Energy and Buildings, Volume 43, Issue 9, September 2011, Pages 2509-2517, ISSN 0378-7788, http://dx.doi.org/10.1016/j.enbuild.2011.06.004.

[21] Guobing Zhou, Yongping Yang, Hong Xu, Performance of shape-stabilized phase change material wallboard with periodical outside heat flux waves, Applied Energy, Volume 88, Issue 6, June 2011, Pages 2113-2121, ISSN 0306-2619, http://dx.doi.org/10.1016/j.apenergy.2011.01.016.

[22] Guobing Zhou, Yongping Yang, Xin Wang, Jinming Cheng, Thermal characteristics of shape-stabilized phase change material wallboard with periodical outside temperature waves, Applied Energy, Volume 87, Issue 8, August 2010, Pages 2666-2672, ISSN 0306-2619, http://dx.doi.org/10.1016/j.apenergy.2010.02.001.

[23] Naser P. Sharifi, Ahsan Aadil Nizam Shaikh, Aaron R. Sakulich, Application of phase change materials in gypsum boards to meet building energy conservation goals, Energy and Buildings, Volume 138, 1 March 2017, Pages 455-467, ISSN 0378-7788, http://dx.doi.org/10.1016/j.enbuild.2016.12.046.

[24] Haoshu Ling, Chao Chen, Hong Qin, Shen Wei, Jie Lin, Na Li, Mingxing Zhang, Nan Yu, Yin Li, Indicators evaluating thermal inertia performance of envelops with phase change material, Energy and Buildings, Volume 122, 15 June 2016, Pages 175-184, ISSN 0378-7788, http://dx.doi.org/10.1016/j.enbuild.2016.04.009.

[25] G. Evola, L. Marletta, F. Sicurella, A methodology for investigating the effectiveness of PCM wallboards for summer thermal comfort in buildings, Building and Environment, Volume 59, January 2013, Pages 517-527, ISSN 0360-1323, http://dx.doi.org/10.1016/j.buildenv.2012.09.021.

[26] Hong Ye, Linshuang Long, Haitao Zhang, Ruqiang Zou, The performance evaluation of shape-stabilized phase change materials in building applications using energy saving index, Applied Energy, Volume 113, January 2014, Pages 1118-1126, ISSN 0306-2619, http://dx.doi.org/10.1016/j.apenergy.2013.08.067.

[27] Xiaoqin Sun, Quan Zhang, Mario A. Medina, Kyoung Ok Lee, Shuguang Liao, Parameter design for a phase change material board installed on the inner surface of building exterior envelopes for cooling in China, Energy Conversion and Management, Volume 120, 15 July 2016, Pages 100-108, ISSN 0196-8904, http://dx.doi.org/10.1016/j.enconman.2016.04.096.

[28] Jiawei Lei, Jinglei Yang, En-Hua Yang, Energy performance of building envelopes integrated with phase change materials for cooling load reduction in tropical Singapore, Applied Energy, Volume 162, 15 January 2016, Pages 207-217, ISSN 0306-2619, http://dx.doi.org/10.1016/j.apenergy.2015.10.031.

[29] Stephen D. Zwanzig, Yongsheng Lian, Ellen G. Brehob, Numerical simulation of phase change material composite wallboard in a multi-layered building envelope, Energy Conversion and Management, Volume 69, May 2013, Pages 27-40, ISSN 0196-8904, http://dx.doi.org/10.1016/j.enconman.2013.02.003.

[30] Frédéric Kuznik, Joseph Virgone, Experimental assessment of a phase change material for wall building use, Applied Energy, Volume 86, Issue 10, October 2009, Pages 2038-2046, ISSN 0306-2619, http://dx.doi.org/10.1016/j.apenergy.2009.01.004.

[31] I. Mandilaras, M. Stamatiadou, D. Katsourinis, G. Zannis, M. Founti, Experimental thermal characterization of a Mediterranean residential building with PCM gypsum board walls, Building and Environment, Volume 61, March 2013, Pages 93-103, ISSN 0360-1323, http://dx.doi.org/10.1016/j.buildenv.2012.12.007.

[32] Luisa F. Cabeza, Cecilia Castellón, Miquel Nogués, Marc Medrano, Ron Leppers, Oihana Zubillaga, Use of microencapsulated PCM in concrete walls for energy savings, Energy and Buildings, Volume 39, Issue 2, February 2007, Pages 113-119, ISSN 0378-7788, http://dx.doi.org/10.1016/j.enbuild.2006.03.030.

[33] Dong Li, Yumeng Zheng, Changyu Liu, Guozhong Wu, Numerical analysis on thermal performance of roof contained PCM of a single residential building, Energy Conversion and Management, Volume 100, August 2015, Pages 147-156, ISSN 0196-8904, http://dx.doi.org/10.1016/j.enconman.2015.05.014.

[34] Francesco Guarino, Andreas Athienitis, Maurizio Cellura, Diane Bastien, PCM thermal storage design in buildings: Experimental studies and applications to solaria in cold climates, Applied Energy, Volume 185, Part 1, 1 January 2017, Pages 95-106, ISSN 0306-2619, http://dx.doi.org/10.1016/j.apenergy.2016.10.046.

[35] Alexander M. Thiele, Gaurav Sant, Laurent Pilon, Diurnal thermal analysis of microencapsulated PCM-concrete composite walls, Energy Conversion and Management, Volume 93, 15 March 2015, Pages 215-227, ISSN 0196-8904, http://dx.doi.org/10.1016/j.enconman.2014.12.078.
[36] Domenico Mazzeo, Giuseppe Oliveti, Natale Arcuri, Multiple Bi-phase Interfaces in a PCM Layer Subject to Periodic Boundary Conditions Characteristic of Building External Walls, Energy Procedia, Volume 82, December 2015, Pages 472-479.
[37] D. Mazzeo, G. Oliveti, M. De Simone, N. Arcuri, Analytical model for solidification and melting in a finite PCM in steady periodic regime, International Journal of Heat and Mass Transfer, Volume 88, September 2015, Pages 844-861.
[38] UNI 10349:1994. Heating and cooling of buildings. Climatic data.
[39] Solar Energy Laboratory University of Wisconsin-Madison, TRNSYS, Version 17, 2012.
[40] EN ISO 13790:2008. Energy performance of buildings – calculation of energy use for space heating and cooling
[41] UNI TS 11300-1:2008. Energy performance of buildings. Part 1: Evaluation of energy need for space heating and cooling.
[42] EN ISO 6946:1997. Building components and building elements – Thermal resistance and thermal transmittance – Calculation method.
[43] Oliveti G, Arcuri N, De Simone M, Bruno R. Experimental evaluations of the building shell radiant exchange in clear sky conditions. Solar Energy 2012; 86:1785-1795.

Highlights

- A set of parameters for a complete thermal characterization of PCM layers are defined
- Various PCM layers with different melting temperatures are considered
- The analysis regard a continental and a mediterranean climate
- Dynamic parameters are related to the latent storage efficiency
- Phase change in the 35% of the layer thickness is sufficient to reach high thermal performances

List of Figure Captions

Figure1

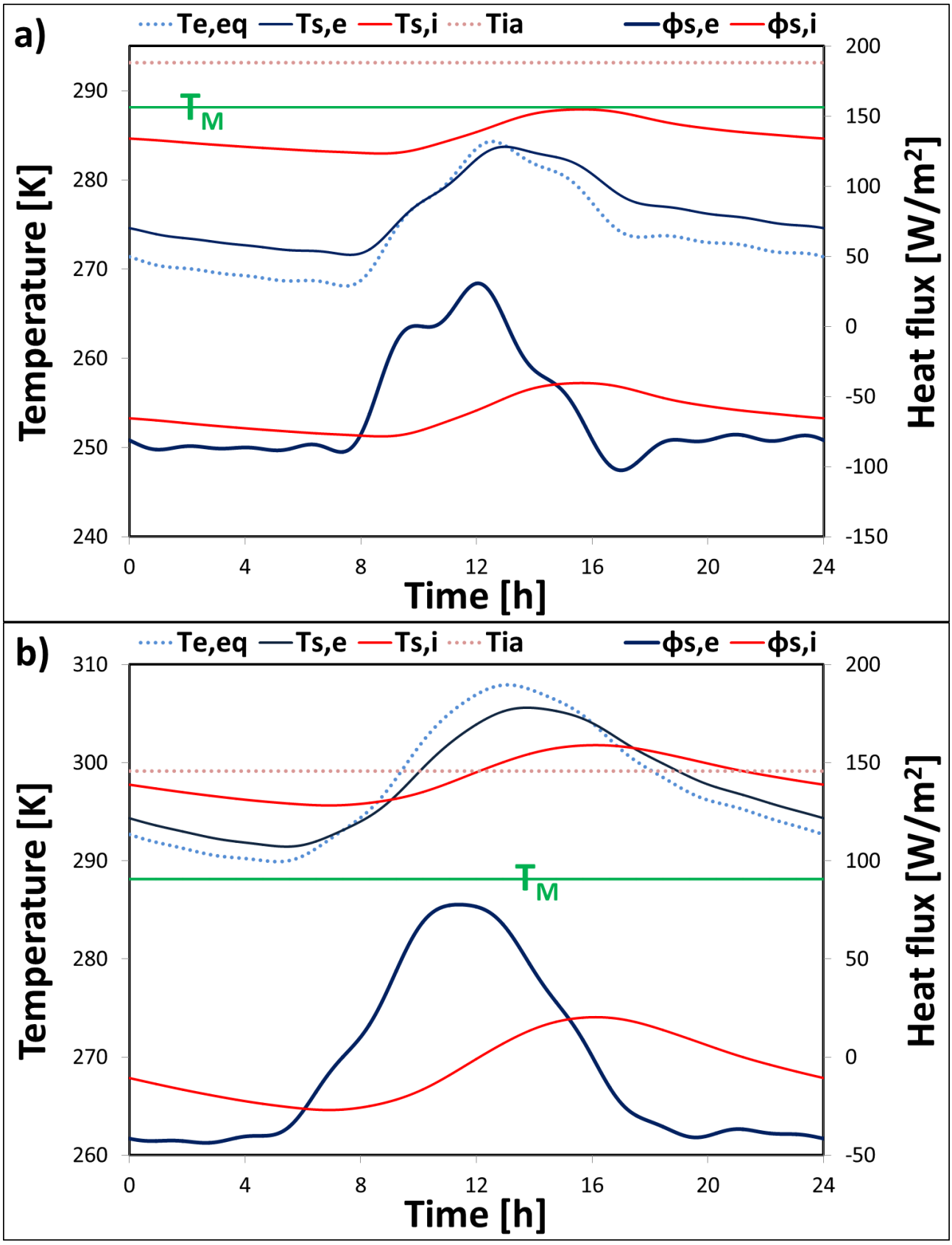
a)
Te,eq
Ts,e
Ts,i
Tia
ϕs,e
ϕs,i
T_M
Temperature [K]
Heat flux [W/m²]
Time [h]
b)
Te,eq
Ts,e
Ts,i
Tia
ϕs,e
ϕs,i
T_M
Temperature [K]
Heat flux [W/m²]
Time [h]

Figure2

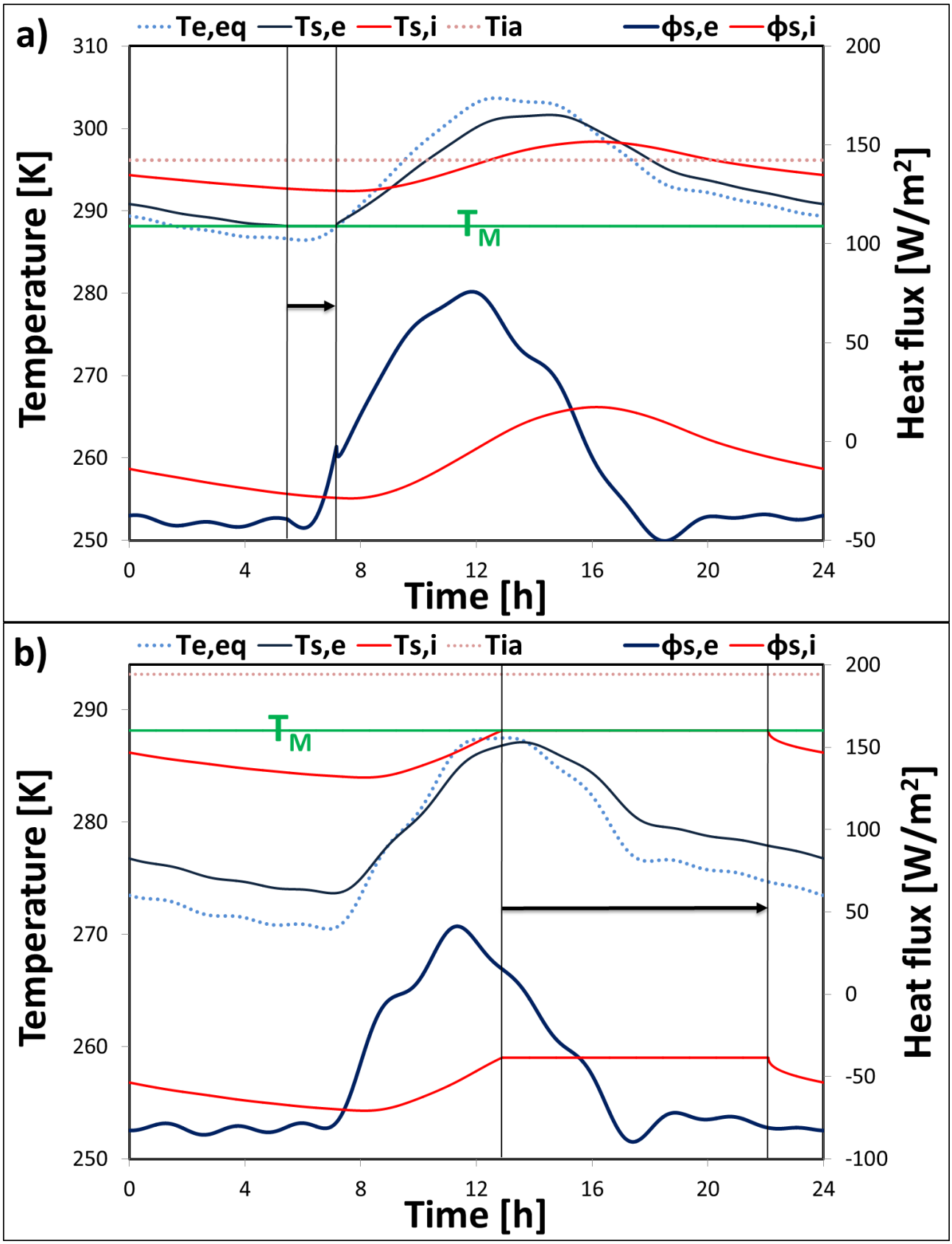
a)
Te,eq
Ts,e
Ts,i
Tia
ϕs,e
ϕs,i
Temperature [K]
Heat flux [W/m²]
Time [h]
T_M
b)
Te,eq
Ts,e
Ts,i
Tia
ϕs,e
ϕs,i
Temperature [K]
Heat flux [W/m²]
Time [h]
T_M

Figure3

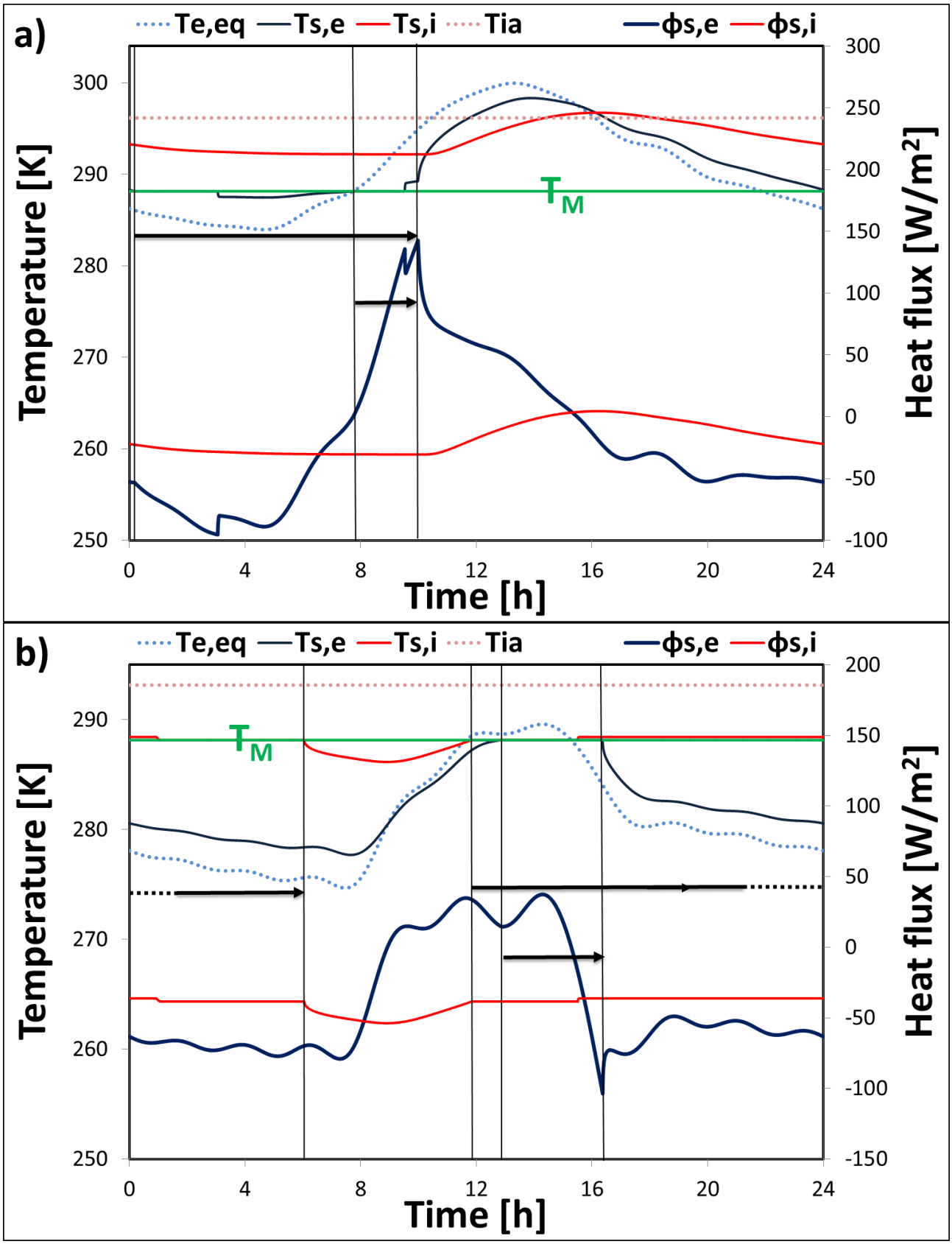
a)
Te,eq
Ts,e
Ts,i
Tia
ϕs,e
ϕs,i
Temperature [K]
Heat flux [W/m²]
T_M
Time [h]
b)
Te,eq
Ts,e
Ts,i
Tia
ϕs,e
ϕs,i
Temperature [K]
Heat flux [W/m²]
T_M
Time [h]

Figure4

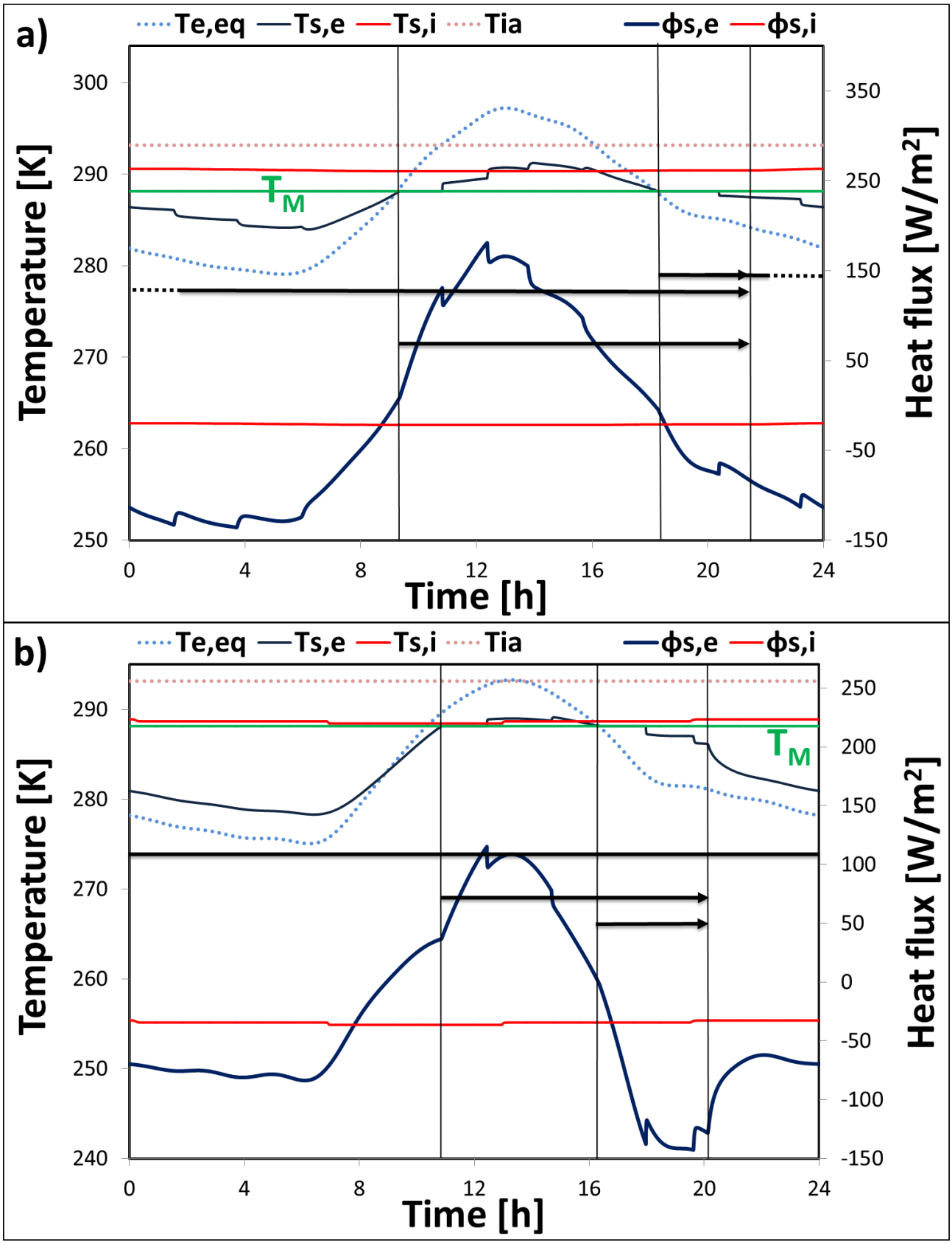
a)
Te,eq
Ts,e
Ts,i
Tia
ϕs,e
ϕs,i
Temperature [K]
Heat flux [W/m²]
T_M
Time [h]
b)
Te,eq
Ts,e
Ts,i
Tia
ϕs,e
ϕs,i
Temperature [K]
Heat flux [W/m²]
T_M
Time [h]

Figure5

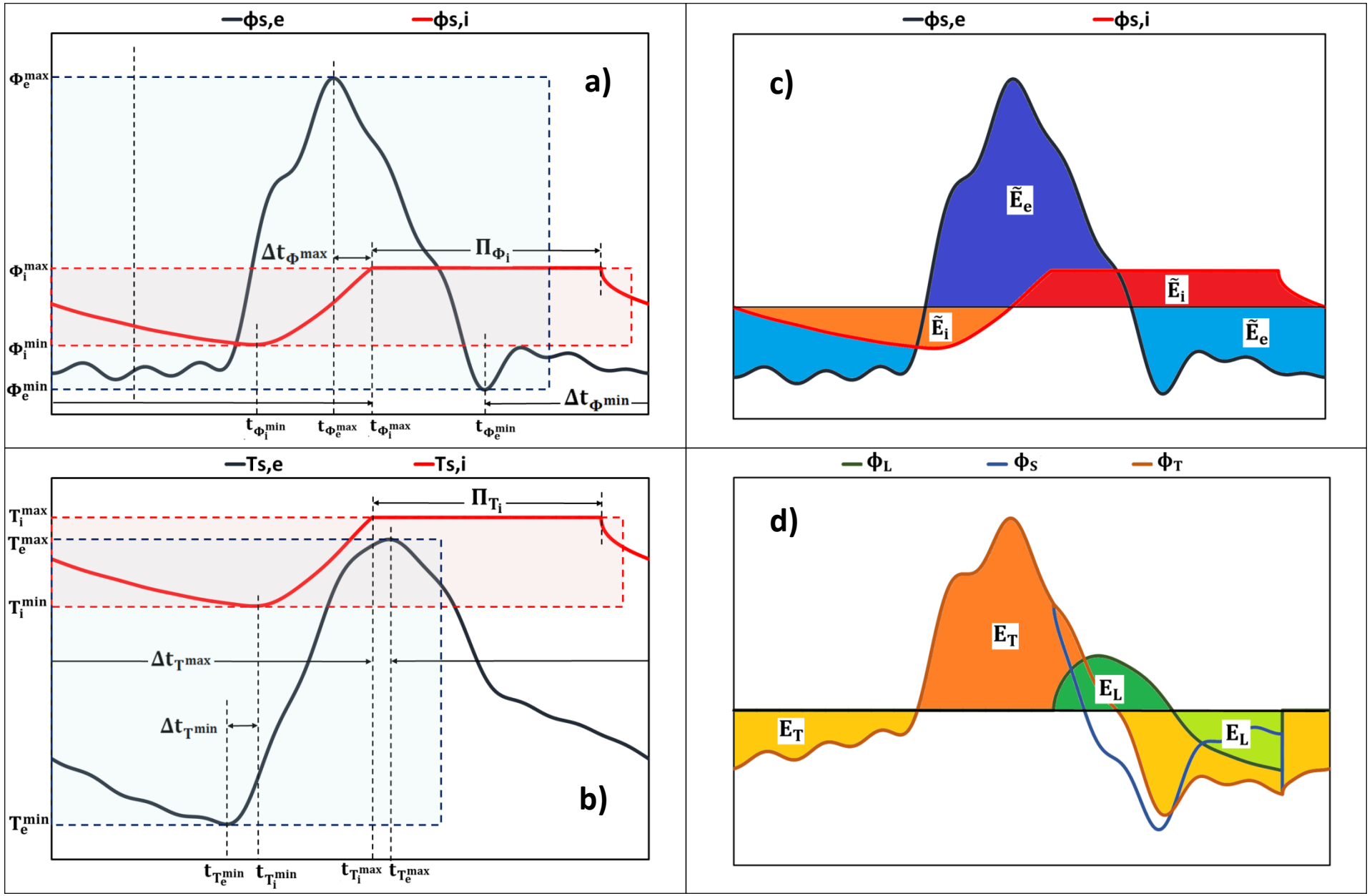
ϕs,e
ϕs,i
a)
Φ_e^{max}
Φ_i^{max}
Φ_i^{min}
Φ_e^{min}
$\Delta t_{\Phi}{}^{max}$
Π_{Φ_i}
$\Delta t_{\Phi}{}^{min}$
$t_{\Phi_i}^{min}$
$t_{\Phi_e}^{max}$
$t_{\Phi_i}^{max}$
$t_{\Phi_e}^{min}$
c)
$\tilde{E}_e$
$\tilde{E}_i$
$\tilde{E}_i$
$\tilde{E}_e$
Ts,e
Ts,i
b)
T_i^{max}
T_e^{max}
T_i^{min}
T_e^{min}
Π_{T_i}
$\Delta t_{T}{}^{max}$
$\Delta t_{T}{}^{min}$
$t_{T_e}^{min}$
$t_{T_i}^{min}$
$t_{T_i}^{max}$
$t_{T_e}^{max}$
ϕ_L
ϕ_S
ϕ_T
d)
E_T
E_T
E_L
E_L

Figure6

		JAN	FEB	MAR	APR	MAY	JUN	JUL	AUG	SEP	OCT	NOV	DEC
S15	N° interface	0	1b	3b	3a	2a	0	0	0	1a	2a	2b	1b
	Phases configuration in the layer	S	S L	S L S L	S L S L	L S L	L	L	L	L S	L S L	L S L	S L
LATEST20	N° interface	0	0	0	2a	3b	2a	1b	2a	2a	2a	0	0
	Phases configuration in the layer	S	S	S	S L S	S L S L	L S L	S L	L S L	L S L	S L S	S	S
HS22P	N° interface	0	0	0	0	1a	2a	2a	2a	2a	0	0	0
	Phases configuration in the layer	S	S	S	S	L S	L S L	L S L	L S L	S L S	S	S	S
SP26	N° interface	0	0	0	0	0	2a	2a	2a	2a	0	0	0
	Phases configuration in the layer	S	S	S	S	S	S L S	S L S	S L S	S L S	S	S	S
C32	N° interface	0	0	0	0	0	0	0	0	0	0	0	0
	Phases configuration in the layer	S	S	S	S	S	S	S	S	S	S	S	S

Figure7

		JAN	FEB	MAR	APR	MAY	JUN	JUL	AUG	SEP	OCT	NOV	DEC
S15	N° interface	3b	3b	3b	2a	2a	0	0	0	0	2a	2a	3b
	Phases configuration in the layer	S L S L	S L S L	S L S L	L S L	L S L	L	L	L	L	L S L	L S L	S L S L
LATEST20	N° interface	0	2a	2a	3b	3b	2a	1a	1a	2a	3b	2a	2a
	Phases configuration in the layer	S	S L S	S L S	S L S L	S L S L	L S L	S L	S L	L S L	S L S L	S L S	S L S
HS22P	N° interface	0	0	0	2a	2a	2a	2a	2a	2a	2a	2a	0
	Phases configuration in the layer	S	S	S	S L S	S L S	L S L	L S L	L S L	L S L	S L S	S L S	S
SP26	N° interface	0	0	0	0	2a	2a	2a	2a	2a	2a	1a	0
	Phases configuration in the layer	S	S	S	S	S L S	S L S	L S L	L S L	S L S	S L S	L S	S
C32	N° interface	0	0	0	0	0	0	2a	2a	2a	0	0	0
	Phases configuration in the layer	S	S	S	S	S	S	S L S	S L S	S L S	S	S	S

Figure8

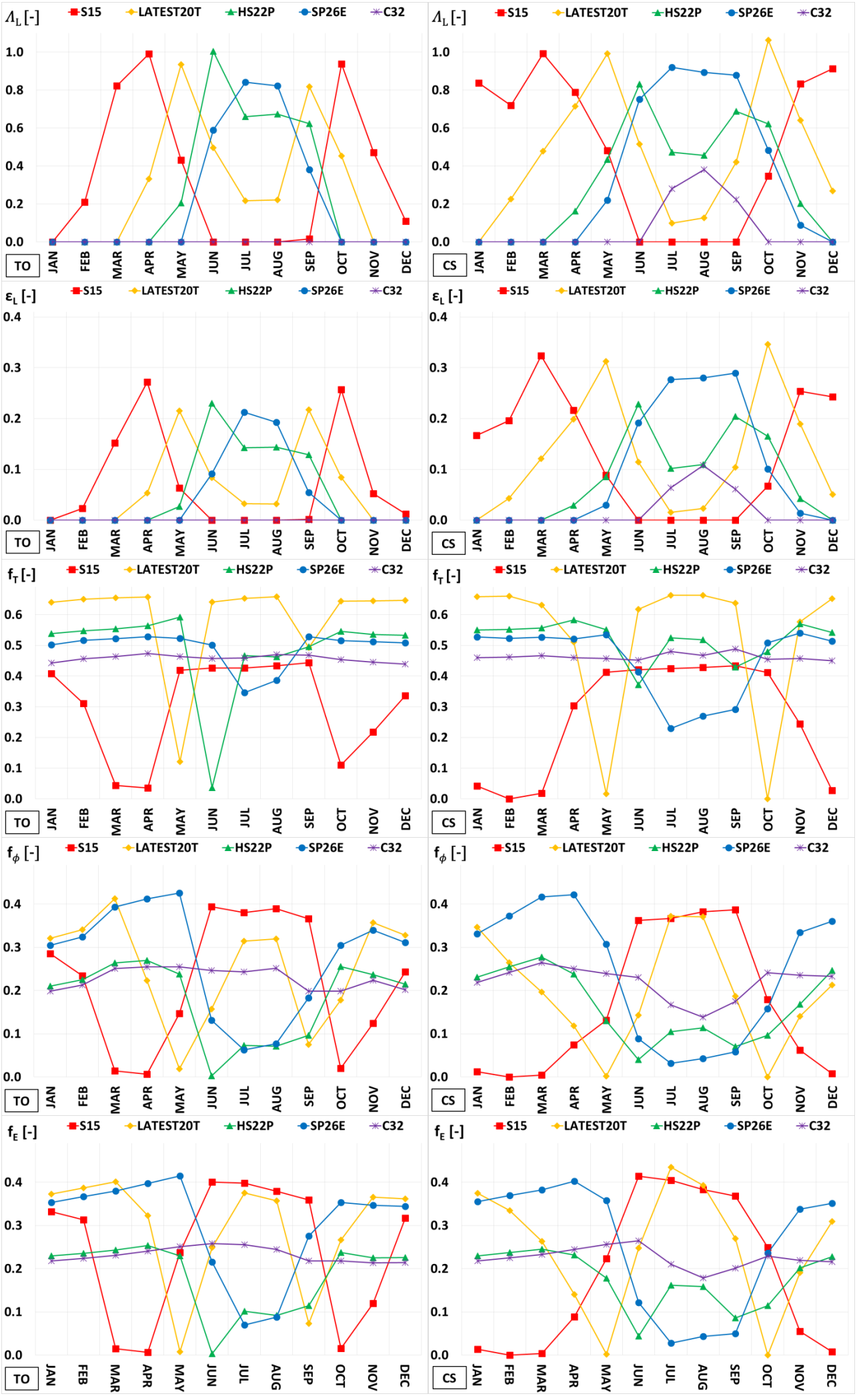
Λ_L [-]
S15
LATEST20T
HS22P
SP26E
C32
TO
CS
ε_L [-]
f_T [-]
f_ϕ [-]
f_E [-]
JAN
FEB
MAR
APR
MAY
JUN
JUL
AUG
SEP
OCT
NOV
DEC

Figure9

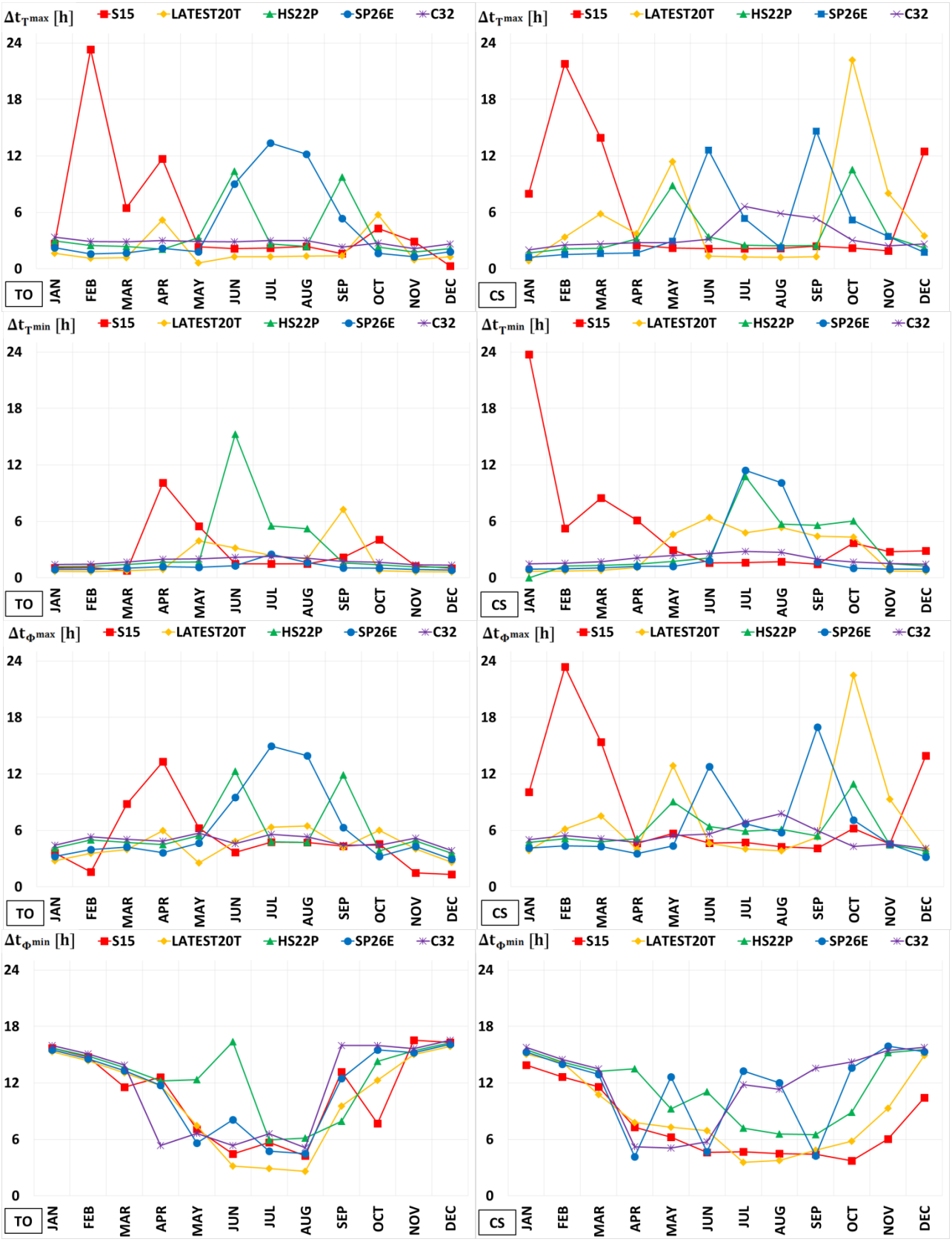
$\Delta t_{T^{max}}$ [h]
S15
LATEST20T
HS22P
SP26E
C32
24
18
12
6
0
TO
CS
JAN
FEB
MAR
APR
MAY
JUN
JUL
AUG
SEP
OCT
NOV
DEC
$\Delta t_{T^{min}}$ [h]
$\Delta t_{\Phi^{max}}$ [h]
$\Delta t_{\Phi^{min}}$ [h]

Figure10

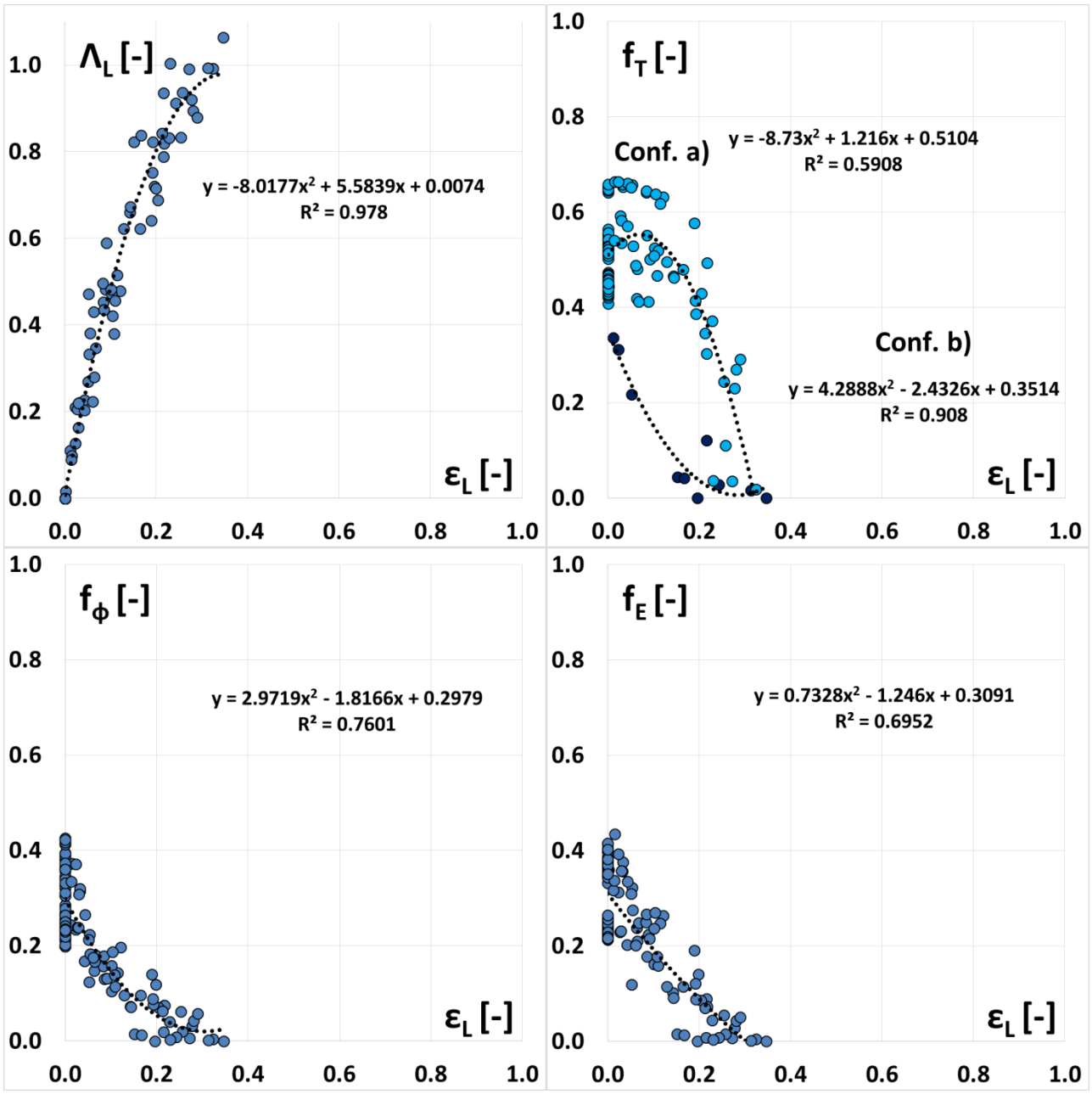
Λ_L [-]
y = -8.0177x² + 5.5839x + 0.0074
R² = 0.978
ε_L [-]
f_T [-]
Conf. a)
y = -8.73x² + 1.216x + 0.5104
R² = 0.5908
Conf. b)
y = 4.2888x² - 2.4326x + 0.3514
R² = 0.908
ε_L [-]
f_ϕ [-]
y = 2.9719x² - 1.8166x + 0.2979
R² = 0.7601
ε_L [-]
f_E [-]
y = 0.7328x² - 1.246x + 0.3091
R² = 0.6952
ε_L [-]

Figure11

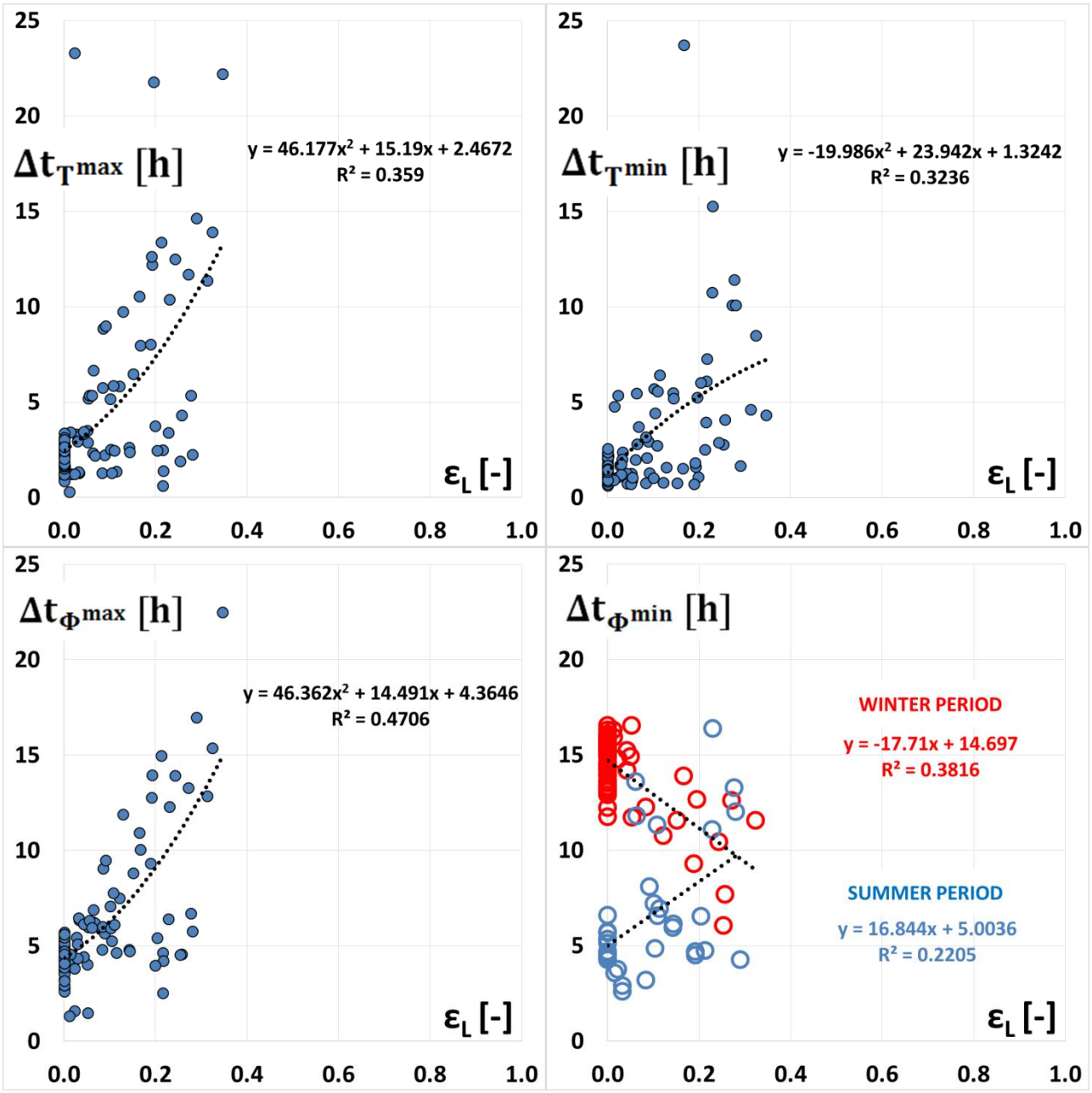
Δt_Tmax [h]
y = 46.177x² + 15.19x + 2.4672
R² = 0.359
ε_L [-]
Δt_Tmin [h]
y = -19.986x² + 23.942x + 1.3242
R² = 0.3236
ε_L [-]
Δt_Φmax [h]
y = 46.362x² + 14.491x + 4.3646
R² = 0.4706
ε_L [-]
Δt_Φmin [h]
WINTER PERIOD
y = -17.71x + 14.697
R² = 0.3816
SUMMER PERIOD
y = 16.844x + 5.0036
R² = 0.2205
ε_L [-]

Figure12

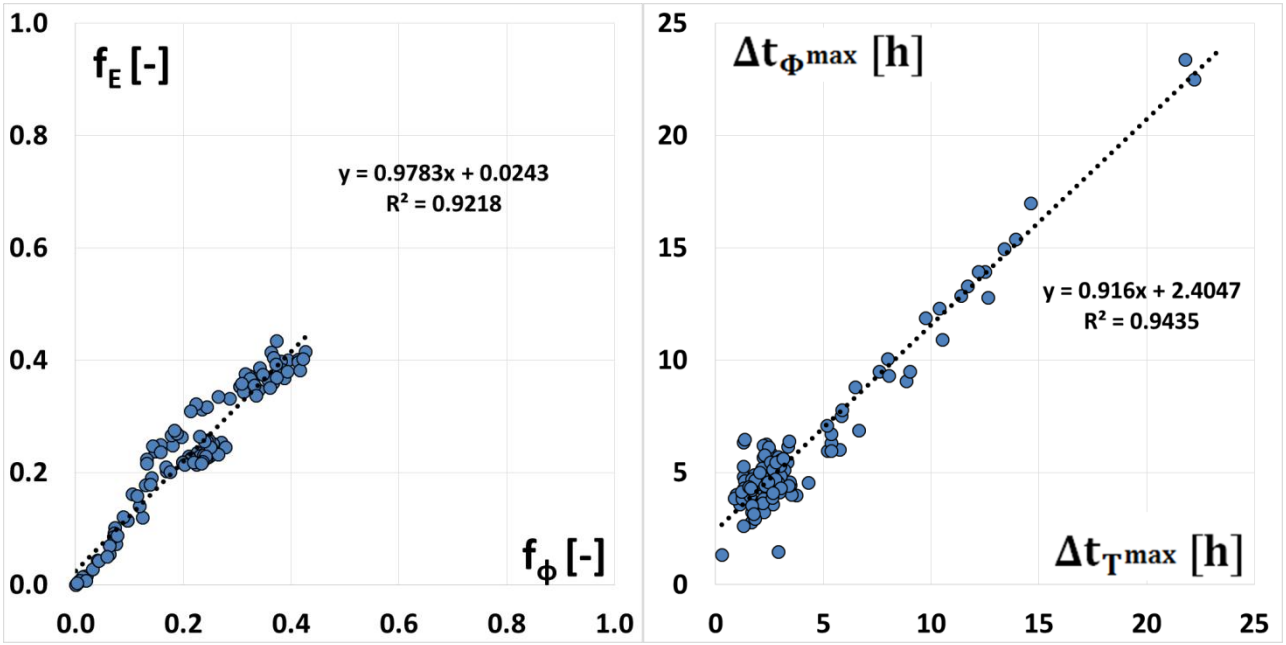
1.0
0.8
0.6
0.4
0.2
0.0
f_E [-]
y = 0.9783x + 0.0243
R² = 0.9218
f_ϕ [-]
0.0
0.2
0.4
0.6
0.8
1.0
25
20
15
10
5
0
$\Delta t_{\Phi max}$ [h]
y = 0.916x + 2.4047
R² = 0.9435
$\Delta t_{T max}$ [h]
0
5
10
15
20
25

Table 1 with Caption

Table 1 - Description of the dynamic behavior of a PCM layer in some special cases and related latent storage parameter values, ε_L and Λ_L and of the constant peak time fractions Π_{T_i} and Π_{Φ_i}.

Case 1	$\varepsilon_L = 0$	$\Lambda_L = 0$	$\Pi_{T_i} = 0$	$\Pi_{\Phi_i} = 0$
Since	The layer is not subject to phase change	The thermal storage is of only sensible energy	The temperature and heat flux are fluctuating on the internal surface	
Then	In order to have phase change, a PCM with a melting temperature higher is required if the layer is in a liquid phase and lower if it is in a solid phase.			
Case 2	$\varepsilon_L = 1$	$\Lambda_L = 1$	$\Pi_{T_i} = 1$	$\Pi_{\Phi_i} = 1$
Since	The whole layer is subject to phase change	The thermal storage is of only latent energy	The thermal fluctuations appear completely dumped on the internal surface	
Then	The layer is thermally well sized.			
Case 3	$0 < \varepsilon_L < 1$	$0 < \Lambda_L < 1$	$\Pi_{T_i} = 1$	$\Pi_{\Phi_i} = 1$
Since	A portion of the layer is subject to phase change and it stores latent energy	The remaining part of the layer is in excess and it only stores sensible energy	The thermal fluctuations appear completely dumped on the internal surface	
Then	A lower PCM thickness is required.			
Case 4	$\varepsilon_L = 1$	$\Lambda_L = 1$	$0 < \Pi_{T_i} < 1$	$0 < \Pi_{\Phi_i} < 1$
Since	The whole layer is subject to phase change	The thermal storage is of only latent energy	The thermal fluctuations appear not to be completely damped on the internal surface	
Then	A higher layer thickness is required.			
Case 5	$0 < \varepsilon_L < 1$	$\Lambda_L \simeq 1$	$0 < \Pi_{T_i} < 1$	$0 < \Pi_{\Phi_i} < 1$
Since	A portion of the layer is subject to a phase change and it stores latent energy	The thermal storage is mainly of the latent energy	The thermal fluctuations appear not to be completely damped on the internal surface	
Then	The PCM shows a high latent heat of fusion and a reduced volumetric heat capacity ρc_p.			
Case 6	$\varepsilon_L = 1$	$0 < \Lambda_L < 1$	$0 < \Pi_{T_i} < 1$	$0 < \Pi_{\Phi_i} < 1$
Since	The whole layer is subject to phase change	The thermal storage is partly sensible and partly latent	The thermal fluctuations appear not to be completely damped on the internal surface	
Then	The PCM shows a reduced latent heat of fusion and a high volumetric heat capacity ρc_p.			

Table2 with Caption

Table 2 – Thermophysical properties of the different types of PCMs.

Company	PCM	Melting temperature T_M [°C]	Heat latent of fusion H [kJ/kg]	Density ρ [kg/m^3]	Thermal conductivity k [W/(m K)]	Specific heat capacity c_p [J/(kg K)]
EPS	S15	15	160	1510	0.43	1900
TEAP	LATEST 20T	20	175	1490	1	2000
savENRG	HS22P	23	185	1690	0.815	3060
RUBITHERM	SP26E	26	190	1450	0.6	2000
CLIMATOR	C32	32	162	1420	0.6	3600

Table 3 with Caption

Table 3 - Monthly average daily values of a whole year of the external air temperature T_{ea} and solar irradiation on the horizontal plane G in Turin and Cosenza.

TURIN (Lat = 45° 7', Long = 7° 43', TO)												
Months	*Jan*	*Feb*	*Mar*	*Apr*	*May*	*Jun*	*Jul*	*Aug*	*Sep*	*Oct*	*Nov*	*Dec*
G [MJ/m^2]	5	7.8	12.2	17	19.6	21.5	23.5	18.5	13.5	9.3	5.5	4.7
T_{ea} [°C]	0.4	3.2	8.2	12.5	16.7	21.1	23.3	22.6	18.8	12.6	6.8	2
COSENZA (Lat = 37° 30', Long = 15° 05', CS)												
Months	*Jan*	*Feb*	*Mar*	*Apr*	*May*	*Jun*	*Jul*	*Aug*	*Sep*	*Oct*	*Nov*	*Dec*
G [MJ/m^2]	7.7	11.8	17.3	21.8	25.7	29.6	28.9	26	20	12.9	9.4	7.7
T_{ea} [°C]	8.1	8.8	11.3	14.4	18.1	23.1	26	25.8	22.7	17.8	13.4	9.4

Table4 with Caption

Table 4 - Indoor environment set point temperature in the different months for Turin and Cosenza.

Indoor environment set point temperature [°C]												
Months	*Jan*	*Feb*	*Mar*	*Apr*	*May*	*Jun*	*Jul*	*Aug*	*Sep*	*Oct*	*Nov*	*Dec*
Turin	20	20	20	20	23	26	26	26	23	20	20	20
Cosenza	20	20	20	23	23	26	26	26	26	23	20	20

Table5 with Caption

Table 5 - Constant peak time fraction $\Pi_{T_i} = \Pi_{\Phi_i}$ during the different months for Turin and Cosenza.

$\Pi_{T_i} = \Pi_{\Phi_i}$	JAN	FEB	MAR	APR	MAY	JUN	JUL	AUG	SEP	OCT	NOV	DEC
S15-TO	0	0.384	0.361	0	0	0	0	0	0	0	0.382	0.235
S15-CS	0.323	1	0	0	0	0	0	0	0	0	0	0.149
LATEST20T-TO	0	0	0	0	0.580	0	0	0	0	0	0	0
LATEST20T-CS	0	0	0	0.351	0.137	0	0	0	0	1	0	0

Data in Brief

Click here to download Data in Brief: Data in Brief.zip